Contrasting roles for two conserved arginines: stabilizing flavin semiquinone or quaternary structure, in bifurcating electron transfer flavoproteins.

Nishya Mohamed-Raseek[1] and Anne-Frances Miller[1,*]

[1] Dept of Chemistry, University of Kentucky, Lexington KY 40506-0055 U.S.A.

* to whom correspondence should be addressed: afmill3r2@gmail.com

Running Title: Contrasting conserved Arg-flavin interactions.

Key Words: electron bifurcation, redox tuning, electron transfer, flavoprotein, flavin, flavin adenine dinucleotide (FAD), site-directed mutagenesis, energy efficiency, domain interface, conformational change.

Abstract

Bifurcating electron transfer flavoproteins (Bf ETFs) are important redox enzymes that contain two flavin adenine dinucleotide (FAD) cofactors, with contrasting reactivities and complementary roles in electron bifurcation. However, for both the 'electron transfer' (ET) and the 'bifurcating' (Bf) FADs, the only charged amino acid within 5 Å of the flavin is a conserved arginine (Arg) residue. To understand how the two sites produce different reactivities utilizing the same residue, we investigated the consequences of replacing each of the Arg residues with lysine, glutamine, histidine, or alanine. We show that absence of a positive charge in the ET site diminishes accumulation of the anionic semiquinone (ASQ) that enables the ET flavin to act as a single electron carrier, due to depression of the oxidized vs. ASQ reduction midpoint potential, $E°_{OX/ASQ}$. Perturbation of the ET site also affected the remote Bf site, whereas abrogation of Bf FAD binding caused chemical modification of the ET flavin. In the Bf site, removal of the positive charge impaired binding of FAD or AMP, resulting in unstable protein. Based on pH dependence, we propose that the Bf site Arg interacts with the phosphate(s) of Bf FAD or AMP, bridging

the domain interface via a conserved peptide loop ('zipper') and favoring nucleotide binding. We further propose a model that rationalizes conservation of the Bf site Arg even in non-Bf ETFs, as well as AMP's stabilizing role in the latter, and provides a mechanism for coupling Bf flavin redox changes to domain-scale motion.

Introduction

Electron transfer flavoproteins (ETFs) are heterodimeric proteins whose fold is described by three domains (Figure 1). The EtfA monomer includes domains I and II while domain III derives from the EtfB monomer. Domain II has been shown to reorient by some 80° relative to the base comprised of domains I and III (1,2), and this conformational change has been proposed to gate electron transfer between the flavins of Bf ETF in the course of turnover (Supporting Figure S1 and (3,4)).

The canonical ETFs were discovered first, in mitochondria, and employ a single FAD to mediate single-electron transfer from client CoA dehydrogenases to the quinone pool via an ETF quinone oxidoreductase, at relatively high reduction midpoint potentials (*E*°s) (5-11). More recently, research has focused on a second clade of ETFs containing two FADs (12) and mediating electron bifurcation (13-15). In this, NADH donates a pair of electrons to the ETF-mediated bifurcation reaction, and in this case a client CoA dehydrogenase may be a high-potential *acceptor,* of one electron. This exothermic electron transfer (ET) reaction is used to drive endothermic transfer of the other electron to a lower potential (more reducing) acceptor: ferredoxin or flavodoxin semiquinone. The Bf ETFs that support nitrogen fixation were named FixAB on this basis (8,13,16,17), and employ a quinone reductase comprised of subunits FixC and FixX as an exergonic acceptor. The FAD that accepts a pair of electrons (2e) from NADH and dispenses them to separate paths is called the bifurcating FAD (Bf FAD, green in Figure 1), whereas the flavin analogous to that of canonical ETFs is called the ET FAD (yellow in Figure 1). It is critical that the ET FAD mediate single electron (1e) only, as exergonic transfer of both electrons would dissipate the reducing energy inherent in NADH. The flavin moiety of the Bf FAD is bound between domains I and III while its AMP portion replaces the AMP of canonical ETFs (18).

Figure 1: Ribbon diagram of RpaETF, details of flavin sites, and the bifurcation reaction.

Working with the Bf ETF of *Rhodopseudomonas palustris* (*Rpa*ETF) Duan *et al.* demonstrated that the two FADs satisfy the thermodynamic requirements for electron bifurcation (19). Specifically, the ET FAD should have two high-potential 1e $E°$'s suiting it to transfer electrons one at a time between the Bf FAD and the FixCX (Figure 1). Thus, the ET FAD should be able to adopt a semiquinone (SQ) state and cycle between it and either the oxidized (OX) state or the fully reduced hydroquinone (HQ) state. Indeed, the ET FAD was observed to accumulate in the anionic SQ state (ASQ) part-way through reductive titrations (10,14,20).

In contrast, the Bf FAD should have a single 2e couple with a lower $E°$, between those of NADH and the ET FAD (21). This too was documented in Bf ETFs from *R. palustris* (19), *Megasphaera elsdenii* (*Mel*ETF) (14), *Pyrobaculum aerophilum* (*Pae*ETF) (22) and *Acidaminococcus fermentans* (*Afe*ETF) (23). The structural identities of the two FADs were deduced based on the analogy of one with canonical ETFs' FAD, in conjunction with binding of NADH near the other (18). Experimental tests characterized flavin known to reside in domain II, based on mutagenesis to replace threonine 94 and 97 that hydrogen bond (H-bond) to ribose of the FAD between domains I and III (T94,97A-*Rpa*ETF), as well as computation to model each flavin's visible spectrum based on its environment in the protein (24). These site-specific approaches confirmed the structural models in assigning functions to each of the flavins in *Rpa*ETF (Figure 1).

Given the contrasting reactivities of the two flavins, it was expected that their two binding sites would be different too, as non-covalent interactions with their protein surroundings are believed to modulate the reactivity of bound flavins (20,25-27). There are, indeed, differences. However, from an electrostatic standpoint, both sites are dominated by an Arg residue that is highly conserved. Since the Arg residues of interest both derive from the A subunit of ETF, we omit the chain specifier and name them by their residue numbers alone. Residue 273 in the ET site is conserved as Arg in 202 of 216 sequences of Bf ETFs and lysine (Lys) in 10 of them, whereas residue 165 in the Bf site is Arg in 214 of 216 Bf ETFs (and Lys in 1) (13). In each case, the Arg is the only charged residue close enough to interact directly with the flavin.

In the case of the ET site, one can rationalize the high $E°$ of the OX/ASQ couple ($E°_{OX/ASQ}$) in terms of a favorable interaction between the anionic SQ formed and the

nearby Arg-273 side chain (10,28). However, it is difficult to rationalize the unstable ASQ in Bf site with the nearby side chain of Arg-165. Not only is the ASQ thermodynamically suppressed, in that it is not seen as an intermediate between OX and HQ in reductive titrations, but its instability (high energy) is understood to be crucial to the Bf flavin's ability to reduce a low-*E*° acceptor (21,29). However, we would expect it to be stabilized by a nearby Arg.

To elucidate the paradox of contrasting reactivities stemming from two flavins presumed to be chemically identical and both in contact with a conserved Arg, we replaced each Arg and characterized the resulting variants' stability, nucleotide content and redox reactivity. Ours are the first biophysical characterizations to our knowledge of Bf ETFs incorporating amino acid substitutions in the Bf site. Our strategy rests on the firm foundation provided by variants of canonical ETFs containing substitutions in the ET site (9,10,28). However, our studies extend the approach to the Arg of the Bf site and demonstrate that the status of each flavin site affects the other. These long-range effects raise the possibility of conformational changes. Indeed, a remarkable 80 ° rotation of domain II relative to the domain I•III base has been documented crystallographically, and is proposed to gate electron transfer in Bf ETFs (3,4) and engage partner proteins (1). With this in mind, we discuss a mechanism suggested by our finding that mutation of Arg-165 abrogates binding not only of FAD, but even AMP in the Bf site. We propose that Arg-165 establishes a network of H-bonds reaching between domains I and III via a conserved peptide loop that bridges between Arg-165 and the phosphate(s) of AMP/FAD. Such a network stabilizing the dimer interface would explain the conservation of Arg-165 even among non-Bf ETFs, and well as retention of AMP as a stabilizer of the quaternary structure (30). It also provides an elegant mechanism by which the oxidation state of the Bf flavin could exert conformational consequences coupling the domain rotation to electron movements.

Results

Flavin content and stability of variants

Considering the ET FAD's unusually stable ASQ state and precedent in canonical ETFs (10,28), it was inferred that a crucial feature of the ET site would be the conserved

Arg-273 that should be positively charged under physiological conditions. However, the Bf ETFs demonstrate that conservation of a nearby Arg does not guarantee a stable ASQ state, as the bifurcating site also contains a conserved Arg, yet suppresses the Bf flavin's SQ states. Thus, the effect appears more nuanced than the identity of the residue, and we expect that the nature of the interaction between Arg and flavin is different in the Bf site than in the ET site. Indeed, Arg-273 is seen in crystal structures to form a π-π stacking interaction with ET FAD (4,18) whereas Arg-165 appears to form bidentate H-bonding interactions with the N5 of Bf FAD and a peptide loop that flanks it (Figure 1C) (31). To test the natures of the interactions, we generated variants which remove the positive charge (replacement with alanine or glutamine, Ala or Gln) or remove bidentate H-bonding (replacement with Lys). We also sought to make the charge tunable via modulation of pH, by replacing Arg-273 with histidine (His). Amino acid substitutions were made in each of the two flavin-binding sites separately.

The variants affecting Arg-273 in the ET site were expressed in soluble form and purified. The yields of 20-25 mg per liter of culture were comparable to that of the WT indicating similarly stable and soluble proteins. Consistent with this, these variants all contained 2 FAD per heterodimer after purification including exposure to 1 mM FAD at the time of cell lysis, to repopulate any FAD binding sites having good affinity (Table 1). Of the variants affecting the Bf site, R165K-*Rpa*ETF behaved like the WT. (Throughout, the R165K notation is used to indicate the variant in which Lys replaces Arg at position 165 of the EtfA.) However, variants lacking a cation in the Bf site displayed lowered affinity for FAD. The R165H-*Rpa*ETF could be purified with close to one bound FAD whereas R165Q-*Rpa*ETF could be purified in low yield with less than one FAD bound at pH 8 (below). R165A-*Rpa*ETF was expressed but partitioned into the insoluble fraction and produced colorless, sparingly stable protein in minute yield.

The T_m values marking the midpoints of thermal denaturation at pH 8 displayed the same trends. Protein secondary structure was monitored via far-UV CD as the temperature was raised. All variants studied displayed similar secondary structure content at 25 °C. The variants that were soluble and readily purified all had T_m values only slightly lower than that of WT. The exception was the R165H-*Rpa*ETF for which the T_m was lower.

Table 1: Flavin contents and thermal stabilities.

Absorbance spectral features

To learn about the environment sensed by the flavins in the modified sites, we compared visible spectra of the variants with those of WT. The absorption bands of the two oxidized flavins overlap almost completely, so for better insight, we exploited the fact that in all variants the ET flavin underwent full reduction before the Bf flavin began to reduce, so a spectrum collected halfway through a reductive titration retained the signature of OX Bf flavin and ET flavin HQ. The difference spectrum from the first half of a titration therefore reflects ET FAD OX minus HQ, and the corresponding difference spectrum for Bf FAD was obtained from the second half of the titration (see Experimental Procedures and Supporting Figure S2). We assumed that the two HQ spectra present in the endpoint spectrum are very similar, and in any case they are weak compared to the OX spectra, especially at longer wavelengths. Therefore, we used the end-point spectrum divided by two as a proxy for either flavin's HQ. Addition of this spectrum to the above difference spectra yielded the deduced OX spectra for the ET flavin and Bf flavin. These are compared in Figure 2 and Table 2. The R165H-*Rpa*ETF and R165Q-*Rpa*ETF variants displayed several distinct properties, so they are discussed together in later sections.

Figure 2: Comparison of visible absorbance spectra of the different variants.

Table 2: Comparison of absorption maxima of individual flavins in each variant, at pH 8.

In all our variants except R165K-*Rpa*ETF the Bf FAD displays vibrational features in band I, and in all cases the two bands are well separated, absorbing around 450 and 370 nm, respectively, with comparable band heights, usually favoring band I. On the other hand, for ET FAD, the separation between bands I and II is smaller producing a shallower dip between them (band II is shifted to 386-392 nm), and the amplitude of band II is higher than or equal to that of band I. Thus the red-shifted band II position of ET FAD in WT-*Rpa*ETF (394 vs. free FAD at 374 nm) resembles that documented for T94,97A (394 nm) (24), *Afe*ETF (~410 nm) (18) and *Mel*ETF 410 nm) (12,32).

Effects on the ET flavin: In response to substitution of Arg-273, the ET flavin's band II was generally more responsive than band I, consistent with the larger change in

molecular dipole associated with band II than band I (33,34). Replacements of Arg-165 in the Bf site also had negligible effects on ET flavin band I's absorption maximum, but absence of Bf FAD and replacement of Arg-165 with His caused the ET flavin's band II to shift significantly in response to this remote change.

The ET flavin's responsiveness to substitutions in either site, including the published T94,97A double substitution, can be rationalized as a consequence of the ET flavin being bound to a mobile head domain that brings the ET flavin close to the base domain in one conformation ('closed' or B-like), but exposes it more in another ('open' or D, Figure S1) (1,4). Thus, the environment of the ET flavin is expected to be affected not only by perturbations that affect the local environment, but also by perturbations of the conformational equilibrium. Our observation of ET flavin spectral changes in response to perturbation of the Bf site are thus consistent with events in the Bf site being coupled to the conformational equilibrium.

Effects on the Bf flavin: The absorption maxima of the Bf flavin both shifted to slightly longer wavelengths in response to replacement of Arg-165 by Lys, despite the retention of positive charge. The 6 nm and 4 nm shifts (band I and band II, respectively), suggest that the interaction between the Arg side chain and the flavin includes mechanisms additional to electrostatics. Indeed, the vibronic structure characterizing the Bf flavin's band I was lost in the R165K-*Rpa*ETF variant, but not variants perturbed in the ET site (see Figure 2 and caption). Because the vibrational structure is a signature of H-bonding (35,36), its loss in R165K-*Rpa*ETF, specifically, suggests that in WT-*Rpa*ETF the flavin H-bonds with Arg-165. Bf FAD's greater sensitivity to local perturbation than displayed by ET flavin is consistent with the lower solvent exposure of the Bf flavin (see Table 2).

Accumulation of ET FAD ASQ in the different ETF variants.

Whereas free FMN in water forms the SQ state in only 1% of the population when the populations of OX and HQ are equal (system is half reduced) (37) the ET site of ETF is remarkable in that almost the entire population assumes the ASQ state when this flavin is half reduced (Figure 3) (20,28). This is critical to the bifurcation mechanism, as it disfavors pairwise transfer of both electrons from NADH to the ET flavin. To test for retention of this property in the Arg variants, we reduced them, stepwise, with sodium

dithionite (NaDT), Ti(III)-citrate, or the xanthine/xanthine oxidase system (38), and measured the maximum extent of ASQ formation between phases 1 and 2 of the reduction.

Figure 3: Reductive titration of R165K-*RpaETF.*

Reduction of all R273-*Rpa*ETF variants and R165K-*Rpa*ETF showed a triphasic reduction (Figure 3). As in previous work on *Rpa*ETF (19), *Mel*ETF (14) and *Afe*ETF (23), reduction first generated an ASQ as indicated by increased absorbance near 374 nm in conjunction with decreased absorbance at 454 nm and an isosbestic around 390 nm. In the second phase, absorbance intensity decreased especially and 374 nm but also at 454 nm indicating formation HQ from ASQ. These phases represent two sequential 1e reductions of a higher-*E*° FAD (ET FAD). Further deflation, in a third phase affecting A_{454} more than A_{374}, revealed 2e reduction of the lower-*E*° FAD (Bf FAD). The absence of detectable SQ at the midpoint of this phase indicates that the Bf FAD has crossed potentials and a suppressed SQ (21).

The R273-*Rpa*ETF variants displayed differences in the maximum amount of ASQ accumulated between phases 1 and 2. The extent of ASQ formation was determined from the slope of the plot of A_{374} vs. A_{454} (inset to Figure 3). The slope early in phase 1 (right edge of inset in Figure 3) reveals the extents to which 1e and 2e reduction contribute to consumption of OX. A second estimate of the fraction of sites undergoing 1e reduction was obtained from the slope late in phase 2. Obtained slopes were compared with slopes derived from authentic cases of 1e or 2e reduction of OX flavin, or 1e or 2e formation of HQ flavin, to obtain the extent to which each process contributed. (Details are in supporting information.) Based on the two values obtained in each case, Table 3 summarizes the extent to which 1e ET occurs, expressed as maximum population of ASQ formed ASQ_{max}, in each of the variants.

Table 3: Maximum population of ASQ in different variants.

Our analysis reveals maximal ASQ accumulation varying from 0.84 (almost all sites) to 0.52. Since an ASQ_{max} of 1/3 is expected when the two 1e *E*°s are equal (see Supporting Information), our variants all retain uncrossed potentials ($E°_{OX/ASQ} > E°_{ASQ/AHQ}$). Thus, interactions additional to those of Arg-273 must participate in

converting the ET flavin from being predominantly a 2e site (as in free flavin, with crossed *E*°s) to a 1e site (uncrossed *E*°s). Nevertheless, the role of Arg-273 is large, as replacement of Arg by Ala almost halves the amount of ASQ that accumulates.

Replacement of Arg-273 with Lys had no effect on ASQ yield confirming that the presence of a positive charge is paramount. Among R273A-*Rpa*ETF and R273H-*Rpa*ETF, the R273H-*Rpa*ETF variant better stabilizes ASQ, possibly acquiring a proton in some fraction of sites in conjunction with flavin reduction. Nevertheless, lowering the pH did not detectably increase the yield of ASQ for R273H-*Rpa*ETF. Similarly, stepwise reduction of R273H-*Rpa*ETF at pH 7 did not result in more ASQ, or visible neutral SQ formation, arguing against proton acquisition by the flavin either. Thus, we have no evidence for outright protonation of His-273 or the flavin in this system, and therefore speculate that the His-273 might replicate H-bonding or π stacking between Arg-273 and flavin ASQ that does not occur in R273A-*Rpa*ETF. It is also possible that R273A-*Rpa*ETF and R273H-*Rpa*ETF have different propensities for the two conformations of ETF, thereby explaining the different amounts of ASQ on the basis of a large-scale factor rather than interactions with the flavin. Either of these explanations is consistent with Sucharitakul's report that binding to partner protein eliminated thermodynamic population of ASQ at the ET site (23).

Replacement of Arg-165 in the Bf site with Lys did not alter the 1e vs. 2e reactivity of the ET flavin, however absence of the Bf flavin from T94,97A-*Rpa*ETF slightly diminished the dominance of 1e reactivity. This small drop in stabilization of ASQ is nevertheless interesting, as it provides a second instance of remote effect of the Bf site on the ET flavin.

Determination of Reduction Midpoint Potentials.

To understand whether diminished yields of ASQ reflect less favorable formation of ASQ, or more favorable consumption, we measured individual *E*°s. Given that several of the variants accumulated significantly substoichiometric amounts of ASQ, the potentials halfway through phases 1 and 2 are not the individual 1e *E*°s, but their average is still the 2e *E*° (39). For each variant, we used the average value of the half-way points, and the separation between 1e *E*°s calculated from the ASQ yield, to obtain the individual 1e *E*°s (see Experimental Procedures).

Phase 1 reduction of WT-, R273K-, R273A- or R273H-*Rpa*ETF was monitored at 454 nm, that of R165K-*Rpa*ETF was monitored at 458 nm. The total change associated with phase 1 was initially treated as representing reduction of a full equivalent of ET flavin from OX to ASQ to calculate the $\log([FAD]_{OX}/[FAD]_{ASQ})$ for plotting vs $\log([DYE]_{OX}/[DYE]_{Red})$ (Figure 4). The resulting log/log plot revealed slopes of 0.5 as anticipated for 1e reductions, consistent with the mathematical treatment used (Experimental Procedures and Supporting Table S1). The intercepts were then used to obtain potentials corresponding to the half-way points of this first reduction (24). Analogous procedures yielded the half-way points of the reduction of ASQ to HQ during co-reduction with Nile blue (Supporting Table S1) based on log/log plot slopes of 0.5 indicative of 1e transfer reactions in all cases. The two half-way points were averaged to obtain the average of the two 1e *E*°s (Table S1).

Figure 4: Log/log plots of populations present during co-reduction of ETF and dye in reductive titration of R165K-*Rpa*ETF*.*

Using the average of the two *E*°s, as well as the separation between them calculated from the maximal yields of ASQ (Table 3), we calculated values for $E°_{OX/ASQ}$ and $E°_{ASQ/HQ}$ at pH 8 for each of the variants (Table 4). Our data indicate no significant difference between the $E°_{OX/ASQ}$ values of R273K-*Rpa*ETF and R165K-*Rpa*ETF, but they are 6-8 mV lower than the value obtained for WT. In contrast, introduction of Ala or His in place of the Arg-273 in the ET site dramatically decreased the $E_{OX/ASQ}$. We surmise that this reflects loss of residue 273's positive charge in conjunction with the fact that the OX/ASQ couple creates anionic flavin, because there is little effect on the $E°_{ASQ/HQ}$ couples which do not change the charge of the flavin.

Table 4: Effects on E°s of replacing the arginine residues.

Whereas replacements of Arg-273 could affect the ET flavin via local effects as well as large-scale conformational change, the Bf flavin would be affected only by conformational change. To determine the $E°_{OX/HQ}$ of Bf FAD, we again used the xanthine/xanthine oxidase system, to drive co-reduction of the Bf flavin with the reference dye safranin O (SO) for R273A-*Rpa*ETF and R273H-*Rpa*ETF, or phenosafranin (PS) for WT-*Rpa*ETF, R273K-*Rpa*ETF and R165K-*Rpa*ETF, in the third

phase of reduction (Figure 3, left-hand side of insert). The slopes obtained from the log/log plots were 1.0 (Figure 4 and Supporting Table S1) and calculated potentials are in Table 4. The Bf $E°_{OX/HQ}$ couples of R273A-*Rpa*ETF and R273H-*Rpa*ETF were 40 mV lower than those of WT-*Rpa*ETF, R273K-*Rpa*ETF and R165K-*Rpa*ETF. Thus, the R273A and R273H substitutions in the ET site exert similar long-range effects on the Bf flavin, possibly by altering the conformational equilibrium.

A Possible Role for Kinetics

Canonical ETF from W3A1 and *Mme*ETF form ASQ but resist further reduction to the HQ state (20,28). This tends to magnify the amount of ASQ observed (9). In our case, since substoichiometric ASQ was observed we were instead concerned that formation of ASQ might be impeded, despite our use of slow reductions via the xanthine/XO system. To directly probe the possibility that our diminished ASQ yields reflect a kinetic barrier to formation of ASQ in R273A-*Rpa*ETF and R273H-*Rpa*ETF, we added an amount of dithionite calculated to yield maximal ASQ and monitored the system for 2-3 hours. Accumulation of ASQ was complete in 2 minutes, after which no further accumulation of ASQ was observed. This argues against kinetic suppression of ASQ formation, and instead indicates that removal of Arg-273's positive charge at the ET site diminishes the amount of ASQ formed via thermodynamic effects.

Behavior specific to the R165H-*Rpa*ETF.

Unexpectedly, the R165H-*Rpa*ETF displayed broad absorbance from 500-750 nm (Figure 2). The rest of the spectrum resembled the ET FAD spectrum more than that of the Bf FAD, on the basis of its shallow dip between bands I and II and its λ_{max} value for band II that is closer to the larger value typical of ET flavin than the shorter value of Bf flavin. (R165H-*Rpa*ETF's band II λ_{max} is 6 nm shorter than the shortest ET flavin value but 8 nm longer than the longest Bf flavin value, Table 2). The long wavelength absorbance was present before reconstitution with FAD, when only one flavin was present (see below), so a single FAD is responsible, and it is the one that co-purifies in this variant. Normally these criteria would identify it as the more tightly bound Bf flavin, but the fact that we had modified the Bf site with the R165H substitution cast this assumption in doubt.

Identity of the FAD retained by R165H-*Rpa*ETF

The long wavelength and breadth of the new absorbance are suggestive of a charge-transfer (CT) interaction, for example with a nearby amino acid side chain or substrate analog (40-42). Since the band is not present in the WT, the introduced His-165 is a candidate participant. However CT with His-165 would require that this variant retain FAD in the Bf site, even though the substitution in the Bf site seems more likely to disrupt Bf flavin binding than ET flavin binding. An alternative interpretation is that the long-wavelength band represents a flavin semiquinone (SQ). This would allow that the retained flavin resides in the ET site, but seems surprising in these air-equilibrated samples.

To learn which flavin is retained in R165H-*Rpa*ETF, we exploited the distinct visible CD of the two flavins. The visible CD of R165H-*Rpa*ETF clearly contains the signature of the ET FAD at short wavelength, but also possesses a weak version of the Bf FAD's signature negative CD at longer wavelengths (425 - 500 nm) (Supporting Figure S3). The simplest interpretation is that considerable ET FAD is present, but some Bf FAD accompanies it. However, the long wavelength CD could also reflect perturbation of the ET flavin's environment, even though the substitution is located in the other domain of the ETF. A similar observation has been reported for human ETF, where mutation of Tyr-16 to Ala in domain III significantly changed the longer wavelength flavin CD for FAD bound in domain II, consistent with Tyr-16 reaching between domains (10).

As an additional test of the presence of Bf FAD in R165H-*Rpa*ETF, it was titrated with NADH, because NADH interacts with the Bf FAD site to reduce the system, whereas ETFs lacking Bf flavin are not subject to reduction by NADH (14,18,24). Upon addition of NADH, R165H-*Rpa*ETF was reduced in a 2e manner initially, but after approximately 10% of the flavin was converted to HQ, the rest of the flavin was unreactive (Figure 5B). Because the long wavelength band did not gain strength in conjunction with reduction of Bf flavin with NADH, we can rule out a CT band between Bf flavin HQ and NAD^+. Full reduction was nevertheless achieved by sodium dithionite, but displayed predominantly two phases, corresponding to phases 1 and 2 based on a plot of A_{374} vs A_{450} (inset of Figure 5A). Thus, some 10% of Bf sites contain FAD, but some 90% of the flavin

present is bound in the ET site based on the fraction of absorbance at 454 nm susceptible to reduction by NADH.

Figure 5: Reductive titrations of R165H-RpaETF with NADH or dithionite.

The reductive titrations also assign the broad long-wavelength band to the ET flavin, as the band was diminished by reduction with dithionite in conjunction with reduction of the ASQ of the ET flavin, in phase 2. Thus, we propose that it reflects the SQ state of a modified flavin, since it is not observed in WT-*Rpa*ETF. The ASQ state of 8-formyl flavin accumulates in air (43) or illumination (44), so it can be present in the starting spectrum.

The ET flavin undergoes chemical modification in the R165Q-*Rpa*ETF and R165H-*Rpa*ETF

The spectrum of R165H-*Rpa*ETF can be better understood with reference to that of R165Q-*Rpa*ETF (Figure 6A). Both of these variants possess substoichiometric flavin and both have similar long-wavelength bands. Thus, by extension of our finding for R165H-*Rpa*ETF, we understand that R165Q-*Rpa*ETF contains predominantly the ET flavin. The spectra of R165Q-*Rpa*ETF differs significantly from the ET flavin spectra of the other variants (Figure 2), but bears resemblance to the ET FAD spectrum of T94,97A-*Rpa*ETF at pH 9 (Figure 6A). Both T94,97A-*Rpa*ETF at pH 9 and R165Q-*Rpa*ETF display the distinctive signature of 8-formyl flavin semiquinone, as documented by Macheroux' team for human ETF (see Figure 4B in their paper (43)). Indeed, mass spectrometric analysis of our T94,97A-, R156H- and R165Q-*Rpa*ETF reveals presence of 8-formyl flavin, and EPR detects a radical consistent with 8-formyl flavin ASQ in R165Q-*Rpa*ETF.

Figure 6: Visible spectra of R165H-RpaETF, R165Q-RpaETF and T94,97A-RpaETF.

Fractional production of 8-formyl flavin can also explain the as-isolated spectrum of R165H-*Rpa*ETF at pH 8 (before incubation with FAD, Figure 6A). This R165H displays a small lump at 425 nm where WT-*Rpa*ETF has a dip between the two flavin bands but 8-formyl flavin ASQ has a sharp peak. The same feature is also seen in R165Q-*Rpa*ETF at pH 8 and T94,97A-*Rpa*ETF at pH 9. 8-formyl flavin ASQ furthermore explains R165H-*Rpa*ETF's broad absorbance from 500 - 700 nm, also prominently

displayed by R165Q-*Rpa*ETF (compare with Figures 4 and 6 of Augustin *et al*. (43). The high $E°_{OX/ASQ}$ of 8-formyl flavin explains the accumulation of this species even in air-equilibrated samples (43,45). The spectra of the released flavins also bear the signatures of modified flavin, in which band I is shifted to a longer wavelength of 462 nm in flavin released from R165Q (Figure 6B). However, we note that the amplitude of band II relative to band I deviates from that expected from pure 8-formyl flavin, indicating that modifications other than or additional to oxidation of the 8-methyl may also be present. Additional work is required to sort out this complicated system, but data in hand demonstrate that the long-wavelength band in R165H-*Rpa*ETF and R165Q-*Rpa*ETF, as well as the unusual spectrum of R165Q-*Rpa*ETF, reflect modification of the ET flavin, substantially to 8-formyl flavin. This appears to affect only a minority of sites in the case R165H-*Rpa*ETF (in which spectra also retain the signature of unmodified flavin), but a majority for R165Q-*Rpa*ETF. Thus, it appears that a positively charged residue 165 in the Bf site and/or presence of the Bf FAD has the long-range effect of preventing modification of the ET flavin.

Formation of 8-formyl flavin is well-known in ETFs which lack the Bf FAD, based on occurrence in human ETF, and T94,97A-*Rpa*ETF at pH 9. Yet these variants retain a positive residue at position 165. Thus, we propose that presence of modified ET flavin is a consequence of the lack of Bf flavin in R165H-*Rpa*ETF and R165Q-*Rpa*ETF, and that the primary effect of the R165H and R165Q substitutions is to disfavor acquisition of Bf FAD. Nevertheless, accumulation of modified flavin is faster in R165Q-*Rpa*ETF than in T94,97A-*Rpa*ETF, suggesting that positive charge at position 165 also plays a role.

The Bf site responds to pH changes

Since Arg or Lys at position 165 enable full FAD content, it appears that His and Gln's lack of positive charge and/or their shorter non-polar stalks is/are responsible for poor FAD binding. To distinguish between these, we examined the pH dependence of FAD content in the R165H-*Rpa*ETF as a means of modulating His-273's charge. At pH 8 only 1 FAD was bound, whereas at pH 9, 1.6 FAD were bound per ETF (Table 5). This is opposite to the behavior one would expect if protonation of His-165 and acquisition of positive charge were required to mediate FAD binding in the Bf site. However, it argues that the shorter stalk of His compared to Lys or Arg is less important.

Table 5: pH dependence of flavin occupancy in Bf site variants.

The pH dependence of FAD content was also tested for the R165Q-*Rpa*ETF to determine whether it pertains to His-165 or something else. Interestingly, even R165Q-*Rpa*ETF contains more FAD at pH 9 than at pH 8. However, both variants remain less stable than WT-*Rpa*ETF or R165K-*Rpa*ETF even at pH 9, consistent with their substoichiometric FAD contents and the location of the Bf flavin at a pivotal location in the interface between domains I and III. This pH dependence in conjunction with the benefit of a cationic Arg or Lys at position 165 suggests that some entity should be deprotonated and anionic for optimal FAD binding. Two candidates are the FAD's pyrophosphate or the isoalloxazine ring itself. The pK_a for deprotonation of the isoalloxazine at N3H is 10.3 for free FAD (46). However because the visible spectrum of the Bf flavin in the WT-*Rpa*ETF and R165K-*Rpa*ETF did not display the strong blue shift in band II reported for flavin deprotonated at N3 (46,47), we infer that the pyrophosphate is most likely the anion whose interaction with Arg-165 favours binding.

Given R165H-*Rpa*ETF and R165Q-*Rpa*ETF's low FAD contents, we assessed the possibility that AMP could be bound in lieu of FAD in the Bf site, as in canonical ETFs (7,48). Because our assay detects the adenine moiety's absorbance at 260 nm, ADP could also be responsible for excess A_{260}, but AMP is deemed more likely because it is the natural ligand of canonical ETFs. For ligands released from R165H-*Rpa*ETF, the ratio of A_{260} to A_{450} was only slightly higher than that of FAD, indicating 0.2 AMP bound per ETF. This contrasts with the situation in T94,97A-*Rpa*ETF where the Bf site is fully populated with AMP (and the ET site is replete with FAD) (24). R165Q-*Rpa*ETF had almost as much AMP, but the FAD content was so low that AMP could have been bound in either site. In the R165H-*Rpa*ETF and R165Q-*Rpa*ETF, the sum of the FAD and AMP stoichiometries was closer to the amount required to populate a single site, the ET site based on our results above. Absence of a nucleotide from the Bf site is consistent with the low stability of the R165H/Q-*Rpa*ETF since canonical ETFs lacking AMP are unstable (30). Because AMP is present in T94,97A-*Rpa*ETF but not R165H-*Rpa*ETF or R165Q-*Rpa*ETF, it appears that a cation at position 165 is needed for AMP binding in the ET site. We propose that favorable electrostatic interaction between cationic residue 165 and the phosphate(s) aid in binding even the AMP of canonical

ETFs, not just the FAD of Bf ETFs. This can explain the high conservation of Arg at this position among ETFs in general.

Discussion

In this study, we explored the roles of two Arg residues that are conserved, one in each flavin-binding site. Nevertheless, the sites produce contrasting flavin reactivity. The salient difference between the two flavins is that the ET flavin undergoes reduction by two sequential 1e steps, whereas the Bf flavin undergoes a single 2e reduction. Therefore, we have characterized the effects on redox reactivity of replacing either Arg-273 in the ET site, or Arg-165 in the Bf site of the *Rpa*ETF.

In both sites, replacement of Arg by similarly charged Lys did not alter *E*°(s) or occupancy of the nearby FAD, however 1e reactivity of the ET flavin was diminished when residue 273 was neutral and nucleotide binding in the Bf site was abrogated when residue 165 was neutral. This demonstrates that in both sites, positive charge at the location of the Arg is a critical element of the protein's interaction with FAD, even though nature and consequences of the interaction are different in the two sites.

Redox tuning of the ET flavin for sequential 1e transfer activity

A mechanism preventing the ET FAD from engaging in 2e redox chemistry is important in both canonical and Bf ETFs, and this is the proposed significance of positive charge at Arg-273, since WT-*Rpa*ETF, R273K-*Rpa*ETF and R165K-*Rpa*ETF (retaining Arg-273) all undergo two sequential 1e reductions. However our data demonstrate that in R273A-*Rpa*ETF and R273H-*Rpa*ETF, OX ET FAD can be directly converted to HQ in a substantial fraction of sites (Table 3). ET FAD sites that accept both electrons from the Bf FAD could mediate wasteful 2e reduction of quinone by NADH, *un*coupled from reduction of flavodoxin/ferredoxin.

Quantitatively, the consequences of removal of Arg-273's positive charge conformed with our expectations and strong literature precedent (summarized in Table 6). The ET flavin's elevated $E°'_{OX/ASQ}$ of -61 mV in WT-*Rpa*ETF, compared to that of free flavin (-313 mV (37)), is by no means unique. Indeed, $E°'_{OX/ASQ}$ is *more* elevated in other Bf ETFs. Arg-273's charge is clearly critical since R273A-*Rpa*ETF's and R273H-*Rpa*ETF's $E°'_{OX/ASQ}$ values are lower by more than 60 mV, showing a 5.8 kJ/mol (1.4 kcal/mol)

lower driving force for reduction of OX to ASQ compared to WT-*Rpa*ETF, R273K-*Rpa*ETF and R165K-*Rpa*ETF. This confirms work by Scrutton and coworkers on *Mme*ETF (9,28,49) where replacement of the Arg corresponding to Arg-273 by an Ala lowered $E°'_{OX/ASQ}$ by 200 mV from +153 mV to -47 mV. In our case the largest effect of replacing Arg-273 was a 76 mV depression of $E°_{OX/ASQ}$ observed upon substitution with Ala. The elevated $E°'_{OX/ASQ}$ of the WT systems can be understood substantially in terms of favorable electrostatic interaction of the formed ASQ. Thus, our data agree well with prior work but are the first to extend it to a Bf ETF, where stabilization of the ET flavin in the ASQ state *in-vivo* would limit it to accepting only a single electron (22,50).

Table 6: Comparison of E°'s of 1 and 2-FAD systems.

In contrast with our findings, work from the teams of Scrutton and Frerman found that replacing the ET site Arg with a Lys decreased the $E°'_{OX/ASQ}$ by 60 mV or more (9,10), but their resulting *E°'*s agree with that of our R273K-*Rpa*ETF (for the corresponding R to K variants, $E°'_{OX/ASQ}$ = -62 mV for *Mme*ETF, -39 mV for human ETF, vs. -69 mV for R273K-*Rpa*ETF). In contrast the WT-*Rpa*ETF's $E°_{OX/ASQ}$ is 80 to 200 mV lower than those of WT-human and WT-*Mme*ETF, suggesting that the Arg-273 in *Rpa*ETF is less supportive of ASQ than the corresponding Args in *Mme*ETF and human ETF. We propose that the anomalous $E°'_{OX/ASQ}$ of our WT ET site reflects incomplete engagement of *Rpa*ETF's Arg-273 with the ASQ flavin under our conditions. Crystal structures show the Arg corresponding to Arg-273 interacting with Glu residues in the partner protein (e.g. Glu 198 in butyryl CoA dehydrogenase (Bcd) of *C. difficile*)(4) or the other ETF domain (2). Thus, Arg-273 is prone to multiple interactions that could dilute its stabilizing effect on the ET flavin ASQ and anionic HQ, depending on the protein conformation. Arg-273's tendency to 'dabble' with residues in other domains or partners could be a cause of the observed dramatic change in the ET flavin's *E°*s when *Afe*ETF has access to its partner Bcd (23).

Coupling between flavin reactivities in the two sites, a role for conformation?

By extending substitutions of Arg-273 to Bf ETFs, we can address the new question of consequences for one flavin site of amino acid substitutions in the other. Some cross-talk is expected because the two flavins must function together. Indeed, studies of pre-

steady-state kinetics revealed that the oxidation state of the ET flavin affects the rate of Bf flavin reduction by NADH, as well as its kinetic isotope effect, in *Afe*ETF (50). Similarly, we found that replacement of Arg-273 with neutral residues depressed $E°_{OX/HQ}$ of the Bf flavin. Conversely, Sato *et al.* found that the ET flavin's optical signature depended on the status of the Bf site (12) and we found that absence of the Bf flavin was associated with a shift to shorter wavelengths of band II of the ET flavin and covalent modification. This was observed even when Arg-165 was retained (as in T94,97A).

Prior work on canonical ETFs concluded that Arg-273 forms interactions stabilizing a 'closed' (=B) conformation of isolated ETF (1) and its mutation to other residues removes a kinetic impediment to full reduction (9). Thus, we speculate that our R273A-*Rpa*ETF and R273H-*Rpa*ETF populate the D conformation more than the WT-*Rpa*ETF does, and infer that the $E°_{OX/HQ}$ of the Bf flavin may be lower in the D conformation than in the B conformation. We note that this would act to reinforce the forward catalysis by disfavoring electron transfer back from the ET flavin to the Bf flavin (but see(23)). The lower $E°'_{OX/HQ}$ of the Bf FAD than the $E°_{ASQ/HQ}$ of the ET FAD is critical for bifurcation, and this is preserved in all our variants.

Regarding ET flavin modification observed when the Bf flavin was absent, proclivity to modification is a long-recognized property of the ET flavin of ETFs (51-54). Indeed, at pH 9 we observed flavin modification in the T94,97A-*Rpa*ETF that retains only the ET FAD (24). Spectra of T94,97A-*Rpa*ETF maintained at pH 9, and of FAD released from it, demonstrated formation of 8-formyl flavin (Figure 6B) as described by Macheroux' team (43). However maintenance of T94,97A-*Rpa*ETF at pH 8 prevented formation of the modified FAD, hence our use of pH 8 in the current work (24) whereas earlier work on *Rpa*ETF has been conducted at pH 9 for stability reasons. Augustin *et al*. found that substitutions favoring the 'open' conformation (=D) accelerated formation of 8-formyl flavin (43). Thus, T94,97A-*Rpa*ETF's greater accumulation of 8-formyl flavin than WT-*Rpa*ETF could indicate a higher population of the open conformation. Canonical ETFs that naturally lack Bf FAD could spend more time in the open conformation where Arg-273 will be less committed to interactions with other side chains and thus more engaged

with the ET FAD ASQ, when partner protein is not present. This would make sense of canonical ETFs' higher $E°'_{OX/ASQ}$s than that of WT-*Rpa*ETF.

Nucleotide binding and stabilization of the dimer interface between domains I and III.

Our replacement of Arg-165 with Lys in *Rpa*ETF yielded protein containing 2 FADs and with a WT-like T_m. However, R165Q-*Rpa*ETF and R165H-*Rpa*ETF incorporated much less FAD plus AMP and were too unstable for measurement of *E*°s and other detailed characterizations. The more extreme substitution, R165A, was expressed into insoluble fractions only and could not be recovered for study. Thus, a positive charge is best at position 165, a polar H-bond enables protein folding but not nucleotide binding, and absence of both positive charge and H-bonding even precludes folding of the protein. The significance of H-bonding by Arg-165 is substantiated by the vibrational structure visible on band I of Bf FAD in WT-*Rpa*ETF, but not in R165K-*Rpa*ETF, indicating destabilization of H-bonding interactions in the variant, even though the Bf flavin is bound. We attribute this to Arg's multifunctional head group that is better able to engage in several H-bonds at once.

Although the instability of the R165H-*Rpa*ETF and R165Q-*Rpa*ETF precluded *E*° measurements, we note that the depressed $E°_{OX/HQ}$ of the Bf flavin in WT-*Rpa*ETF reveals that the anionic HQ and ASQ states, in particular, are strongly destabilized by this site. This has been difficult to reconcile with the fact that a nearby Arg should *favor* formation of the anionic states of the flavin. Since R165H-*Rpa*ETF (and R165Q-*Rpa*ETF) appear to not even bind AMP well (whereas T94,97A-*Rpa*ETF does) we propose that the anion stabilized is actually the phosphate(s) associated with the (di)nucleotide, whether FAD or AMP. Since the AMP portion of FAD is bound in domain III (chain B) whereas Arg-165 extends from domain I (chain A) this interaction would act as a link between domains, consistent with AMP's importance to the assembly of canonical ETFs (30).

Such an interaction between domains appears to be mediated via a stretch of peptide backbone from chain B that would not neutralize Arg-165's charge, but instead would propagate it. The peptide is oriented such as to present carbonyl Os to Arg-165's side chain (31). This in turn constrains the peptide to present its backbone NH groups towards the phosphate(s), acting as a zipper to hold together domains I and III (Figure

7). This electrostatically polarized network of H-bond is seen in the crystal structures of each of the ETFs that has been crystallized (Supporting Figure S4).

Figure 7: Extended electrostatically polarized network of H-bonds bridging the domain interface and mediated by the conserved peptide zipper.

The peptide zipper represents one of the conserved signatures of Bf ETFs (13,55). Considering the four residues shown in Figures 7 and S4 as well as the two flanking residues, D**GDTA**Q (the four depicted are in bold), the percent conservation in a set of 216 sequences of Bf ETFs(13) is 100% D, 95% G, 85% D (with E making up an additional 10%), 100% T, 86% A (with G as an other 11%) and 93% Q (with H as 7%). Meanwhile in 449 sequences of canonical (group 1) ETFs, the corresponding sequence is 100% D, 68% D, 98% D, 36% S, 98% N, 92% Q. The residues remain highly conserved, but differently, with an 'extra' Asp that could play the electrostatic role of the second phosphate of FAD that is absent from AMP in canonical ETFs. The Arg corresponding to Arg-165 remains Arg in 447 of 449 canonical ETFs, with Gln or Ser present in the two outliers.

The peptide zipper appears to interact with both phosphates of FAD, suggesting that it could interact similarly with the AMP that replaces FAD in canonical ETFs. Indeed, the motif is evident in the crystal structures of canonical ETFs (Figure S4)(8), providing an explanation for the importance of AMP to assembly of the ETF subunits (56). Thus, we identify a widely shared conserved structural motif linking the subunits and domains of ETF whereby Arg-165 stabilizes the domain interface in conjunction with the nucleotide, via long-range electrostatics mediated by a highly conserved stretch of peptide backbone (the 'zipper').

The proposed extended interaction stabilizing the domain interface can explain the conservation of Arg-165 even in canonical ETFs that lack FAD, and moreover canonical ETFs' retention of AMP (57). It also provides an alternative explanation for the otherwise baffling conservation of Arg in a site that must destabilize ASQ. However, we speculate there may be important functional significance to the use of this electrostatic mechanism to stabilize a particular conformation of the domain interface. We propose that upon reduction of Bf flavin, after release of NAD^+ when the Bf flavin is anionic HQ, the Bf flavin's charge could supersede that of the more distant phosphates and effectively

capture the Arg, thereby releasing Arg's constraints on the peptide zipper. Indeed, the CryoEM structure displays partial inversion of the polarity of the peptide backbone in the loop, consistent with our proposal, and partial reduction of the Bf flavin by the electron beam (58). The freeing of this protein element could allow domain III to reposition itself relative to domain I, providing a means of coupling the interconversion of B and D conformations to the oxidation state of the Bf flavin.

Thus, besides the H-bond between the side chain of Arg-165 and the oxidized flavin N5 (3,31), we now propose that Arg-165 in domain I interacts with the phosphate(s) of FAD or AMP of domain III via a conserved peptide zipper when the Bf FAD is oxidized. We furthermore speculate that upon Bf FAD reduction, reorganization of these interactions in the dimer interface could precipitate conformational change. If confirmed experimentally, this would be an elegant way to couple acquisition of electrons to domain-scale motion, via electrostatics.

Concluding Remarks

Our study reports consequences of replacing each of the conserved active site Args of a Bf ETF, and provides a first glimpse of the Bf flavin's interactions with a nearby residue. We have demonstrated that Arg-273 plays a vital role in stabilizing ET FAD ASQ relative to OX in a Bf ETF, as in canonical ETFs. However, we note that a divided interaction between Arg-273 and the ET flavin in *Rpa*ETF could explain the latter's lower $E°_{OX/ASQ}$. We find that substitutions of neutral residues for Arg-273 also lower the $E°_{OX/HQ}$ of the Bf flavin, and absence of a flavin in the Bf site hastens modification of the ET flavin, demonstrating coupling between the two sites that may be mediated by conformational equilibria. Finally, we have demonstrated that Arg-165 plays an important role in binding nucleotide in the interface between domains I and III. This is consistent with the crystal structures of Bf ETFs in which Arg-165's side chain not only forms an H-bond with the flavin N5, but also forms interactions bridging the domain interface and anchored by the negatively charged phosphate(s) of AMP or FAD. The long-range electrostatic interaction mediated by H-bonding by a conserved stretch of peptide backbone is also observed in canonical ETFs, explaining the stabilizing role of AMP in canonical ETFs and the universal conservation of Arg-165. Moreover, we

speculate that the use of electrostatics to stabilize the dimer interface serves to make the interface inherently responsive to the oxidation state of the Bf flavin.

Experimental Procedures

Site-directed mutagenesis

Note that the A, B naming of the ETF subunits is opposite to their naming in the Fix convention, such that EtfA is FixB, and *vice versa*. Thus, the *fixA* gene encodes EtfB and *fixB* encodes EtfA. Mutations were introduced into *fixB* augmented with an N-terminal His tag in the pMCSG21 plasmid (spectinomycin resistant) (19). Primers encoding the desired amino acid substitutions were designed using NEB base changer (Supporting Table S2) and employed according to the vendor's recommendations to introduce the mutations via polymerase chain reactions using Q5 High Fidelity DNA polymerase (New England Biolabs, Ipswich MA). The mutated construct encoding EtfA and plasmid encoding native EtfB were transformed into competent Nico21(DE3) *Escherichia coli* (New England Biolabs, Ipswich MA), along with pGro7 (Takara Bio, Mountain View, CA, USA) for co-expression of molecular chaperones GroES/EL. Plasmids expressing *fixB* with mutations encoding the R165H or R165K substitutions were obtained from Dr. H. Diessel Duan.

Protein expression and purification

Cells were grown in 1 l of Terrific Broth supplemented with 20 mg/l riboflavin and 2 mM $MgSO_4$ along with carbenicillin (100 µg/ml), spectinomycin (100 µg/ml), and chloramphenicol (50 µg/ml) at 37 °C, shaking at 250 rpm, to an OD_{600} of ~1-2. After cooling the culture to 18 °C, groES/EL gene expression was induced using 1 mg/ml L-arabinose. After 30 min of growth, ETF gene expression was induced using 0.1 mM isopropyl 1- thio-β-D-galactopyranoside (IPTG). Cultures were then grown for an additional 20 h at 18 °C. Cells were harvested by centrifugation at 4500 rpm, 4 °C for 30 min, and the pellet was stored at 80 °C after washing once in PBS (10 mM Na_2HPO_4, 1.8 mM KH_2PO_4, 137 mM NaCl, 2.7 mM KCl, pH 7.4).

Frozen cell pellet (~ 30 g) was thawed and resuspended in 60 ml of BugBuster (Cat no.70923-4 EMD Millipore, Burlington, MA, USA) containing 1 mM 4-(2-aminoethyl) benzenesulfonyl fluoride hydrochloride (Cat no. 21250, Chem-Impex International,

Wood Dale, IL, USA), 1 mM FAD (Cat. No. 00151, Chem-Impex International, Wood Dale, IL, USA), 2 µl of Benzonase® Nuclease HC (Cat. No. 71205-3, EMD Millipore), and 2 µl of rLysozyme™ solution (Cat. No. 71110-4, EMD Millipore) and further incubated at 4 °C for 2 h with stirring. After centrifugation at 15,000 g for 30 min at 4 °C, the clarified protein solution was mixed with 1.5 ml of pre-equilibrated nickel-nitrilotriacetic acid resin (Cat no.88222, Thermofisher) and incubated at 4 °C with stirring for 30 min. Then the mixture was transferred to a column at 4 °C. After collecting the flow-through, the column was washed with 20 column volumes of 20 mM Tris, pH 7.8, 500 mM KCl containing 20 mM imidazole. Finally, the column was developed with 2 column volumes of 20 mM Tris, pH 7.8, 500 mM KCl containing 100 mM imidazole, and the eluate was collected in three fractions. After SDS-PAGE analysis, fractions containing the purest most concentrated protein were pooled and passed over a 10DG column (Bio-Rad) equilibrated with working buffer (20 mM bis-Tris Propane, pH 8.0, 200 mM KCl, 10% (w/v) glycerol), to remove imidazole. To minimize covalent modification of the ET flavin, the current work was conducted at pH 8 unless stated otherwise. Co-expression of WT-*Rpa*ETF in the presence of chaperone and equilibration of the protein with the Ni-NTA resin for a shortened time interval (24,59) enhanced the yield of ETF by 10-fold compared to previous work (19).

FAD lost during purification was reconstituted by overnight incubation in 1 mM FAD at 4 °C in darkness, followed by gel filtration over a 10DG column to remove unbound FAD. This resulted in protein containing 2 FAD per ETF dimer, although Bf ETFs purified without the two exposures to FAD often possessed as little as 1 (12,18). Proteins were used the same day or flash-frozen in liquid nitrogen and stored at -80 °C for later use. The visible spectra of WT and variants other than R165Q-*Rpa*ETF indicate that they were purified predominantly in the oxidized state.

Determination of protein and flavin concentrations

The protein concentration (µg/ml) was determined using the Pierce 660 nm protein assay with bovine serum albumin as the standard (Thermo Fisher scientific, Waltham, MA). ETF mM concentration was calculated based on the molecular mass of 74,545 Da (19).

To quantify flavin and adenine, individual 1.5 mL microcentrifuge tubes containing 350 µl of ~30 µM ETF in working buffer were wrapped in aluminum foil to exclude light and prevent photochemical transformation of cofactors. Cofactors were released by denaturing the ETF by heating at 100 °C for 10 min after which denatured protein was removed by centrifugation at 14,000 x g for 10 min after cooling the samples. Supernatant was transferred to a quartz cuvette and the optical spectrum was recorded on a HP 8453 spectrophotometer. Absorbance at 450 nm was used to determine the released flavin concentration (ε_{450} = 11.3 mM^{-1} cm^{-1})(14). From this and FAD's (ε_{260} = 35.93 mM^{-1} cm^{-1}) we calculated the absorbance due to FAD at 260 nm. The excess A_{260} was used to determine the concentration of AMP or ADP (ε_{260} = 15.0 mM^{-1} cm^{-1})(30).

Far-UV CD for T_m measurement, and visible CD of the flavins

Far-UV CD spectra of all the variants (17-30 µM) were recorded using a JASCO J-800 series spectropolarimeter from 250 to 190 nm starting at 20 °C in a 0. 2 cm path length quartz cuvette with the following parameters: bandwidth= 1.00 nm, scanning speed = 50 nm min^{-1}, and three accumulations. The molar ellipticity was calculated using the equation, $[\theta] = \theta / (c \times l)$, in which θ is the ellipticity in millidegrees, c is the concentration in mM, and l is the cell path length in cm. CD measurements were taken in working buffer starting from 20 °C to 60 °C at 2 °C intervals.

Visible CD spectra of 98 µM of R165H-*Rpa*ETF and 68 µM of WT-*Rpa*ETF were recorded from 600 to 300 nm at 4 °C in a 1.0 cm path length quartz cuvette with the following parameters: scan speed = 100 nm min^{-1}, bandwidth= 2.00 nm, scanning speed = 100 nm min^{-1}, and three accumulations.

Spectral Deconvolution

Individual spectra of each of the flavins were deduced based on their separate sequential reductions in anaerobic titrations with dithionite. Experimental details follow. Plots of A_{374} vs. A_{454} (or absorbances at appropriate λ_{max} values) were used to identify the last spectrum of phase 2, in which the ET flavin is HQ and the Bf flavin is OX (ET_{HQ}/Bf_{OX}). This was subtracted from the first spectrum when both flavins are OX (ET_{OX}/Bf_{OX}) to yield a difference spectrum from which the contribution of Bf_{OX} is removed, to retain only ET_{OX} minus ET_{HQ} (ET_{OX-HQ} in Figure S2). Separately, the

endpoint spectrum of the titration corresponds to ET_{HQ}/Bf_{HQ} so its subtraction from the spectrum at the end of phase 2 (ET_{HQ}/Bf_{OX}) removes contributions from the ET flavin and retains only the Bf_{OX} minus Bf_{HQ} difference spectrum of the Bf flavin (Bf_{OX-HQ} in Figure S2). To correct for the subtractive contribution of an HQ flavin spectrum in both cases, we exploited the fact that the HQ spectrum is weaker than that of OX except at short wavelengths, so any site-specific differences will have a weaker influence. We therefore divided the endpoint spectrum corresponding to ET_{HQ}/Bf_{HQ} by two to yield the HQ spectrum of a single average flavin and added that to each of the two difference spectra (ET_{OX} minus ET_{HQ}, and Bf_{OX} minus Bf_{HQ}) to deduce ET_{OX} and Bf_{OX}. This method was adopted because it consistently gave flat baselines and did not produce any negative absorbances. Sample spectra from an example are provided as Supporting Figure S2.

Extent of ASQ formation

This determination was also based on reductive titrations in inert atmosphere (described below). The extent of ASQ formation was determined from the slope of the plot of A_{374} vs. A_{454} early in phase 1 since this reveals the extents to which of 1e and 2e reduction contribute to consumption of OX (before enough ASQ accumulates to support a significant contribution from reduction of ASQ to HQ). A second estimate of the fraction of sites undergoing 1e reactivity was obtained from the slope late in phase 2, when reduction of OX to ASQ is no longer significant so the slope represents the combination of 1e reduction of ASQ to HQ and 2e reduction of OX to HQ. The three reference slopes are known from the WT case where the phases are well separated and almost pure. Details are provided in the supporting information, including our correction to account for the 16% of WT sites that undergo 2e reduction.

Reductive titrations

Reductive titrations were performed in inert atmosphere, monitored using a HP 8452A spectrophotometer (Agilent technologies) equipped with an OLIS controller, in an inert atmosphere afforded by a glove box (Belle Technology, Waymouth, UK), using a 1 cm path length self-masking quartz cuvette at 25 °C with the temperature controlled by a Quantum NorthWest Peltier cuvette holder. ETF was reduced by small aliquots

amounting 1 μM sodium dithionite (ε_{315} = 8.04 mM^{-1} cm^{-1})(60). This low concentration provides sufficient driving force to fully reduce the FAD at the pH of 8 (61).

Reduction midpoint potential determinations

To obtain the dense stable data sets needed for accurate determination of reduction midpoint potentials, xanthine oxidase in combination with xanthine (420 μM) was used to provide a slow continuous delivery of reducing equivalents (38). The reaction mixture contained 10 μM MV as a redox mediator, ~20- 30 μM of ETF, and 3-5 μM of an appropriate indicator dye with an *E*° close to that of the ETFs so that the two can equilibrate with one-another during reduction (Supporting Table S3). For example, our initial choice of Methylene blue (MB, *E*°' = 11 mV, 2e/H^+ at pH 7, calculated *E*° = -19 mV at pH 8)(61) proved non-optimal for the current variants, as the *E*°s determined in the presence of MB were ~ -50 mV for WT-, R165K- and R273K-*Rpa*ETF. Whereas for R273A- and R273H-*Rpa*ETF, the $E°_{OX/ASQ}$s around ~ 90 mV at pH 8 were more than 30 mV from MB's potential of -19 mV at pH 8 (see Table S3). In addition, we observed that the last steps of reduction of R273A- and R273H-*Rpa*ETF coincided with formation of significant amounts of MV radical, even before full reduction of the ETF was achieved, suggesting a very low *E*° or slow equilibration with the indicator dye in later steps of reduction. Our final choice of indicator dyes resolved this issue too.

The reaction mixture was in working buffer at pH 8 to suppress covalent modification of the ET flavin (43) and thus ensure that changes observed are attributable to the residue being varied, Arg-273 and Arg-165, not other factors. However, this precluded study of R165H-*Rpa*ETF with both FADs bound. The reaction was initiated by addition of 3-10 nM xanthine oxidase depending on the ETF and *E*° of the phase under investigation. Spectra were recorded every 1 min.

$E°_{OX/ASQ}$ characterizing reduction of OX FAD to ASQ was calculated by relating the extent of reduction of FAD to the extent of concurrent reduction of the reference dye. Conversion of OX to ASQ was quantified based on absorbance changes at 454 nm, while the reduction of the dye was quantified based on loss of absorbance at λ_{max} of the dye.

For WT-*Rpa*ETF, the point in the titration corresponding to the maximum ASQ concentration was identified and treated as the endpoint of the first 1-e reduction and

assigned to full conversion to ASQ based on the agreement between the shape of the spectrum and that of authentic samples of 100% ASQ. Each spectrum up to that point in the titration was converted to a difference spectrum by subtracting the endpoint spectrum, to reveal the remaining OX population. Absorbance at 454 nm was used to find the absorbance change due to reduction of one equivalent of FAD and thereby to calculate the fraction of OX converted to ASQ. $[FAD_{OX}]/[FAD_{ASQ}]$ at each point in the titration was calculated from the fractional populations. Absorbance at λ_{max} of the dye was used to calculate the extent to which oxidized dye, Dye_{OX}, was converted to reduced dye, Dye_{RED}. The ratio of oxidized to reduced dye along with that of the FAD were employed in the Nernst equation,

$$log\left(\frac{[\mathrm{FAD}_{OX}]}{[\mathrm{FAD}_{ASQ}]}\right) = \frac{n_{FAD}}{n_{Dye}} log\left(\frac{[\mathrm{Dye}_{OX}]}{[\mathrm{Dye}_{RED}]}\right) + n_{FAD}\frac{F\left(E^{o}_{Dye} - E^{o}_{FAD}\right)}{2.303RT} \qquad \text{Eq. 1}$$

where n_{FAD}, n_{Dye} denote the number of electrons acquired by the flavin and the dye respectively during the reaction under study, and F, R and T are Faraday's constant, the ideal gas constant, and the temperature, respectively. A plot of $log\left(\frac{[\mathrm{FAD}_{OX}]}{[\mathrm{FAD}_{ASQ}]}\right)$ versus $log\left(\frac{[\mathrm{Dye}_{OX}]}{[\mathrm{Dye}_{RED}]}\right)$, was used to determine n_{FAD} from the known value of $n_{Dye} = 2$ (Supporting Table S1).

The intercept of the plot then permits calculation of $E°_{FAD}$ for the ET $FAD_{OX/ASQ}$.

$$intercept = n_{FAD}\frac{F\left(E^{o}_{Dye} - E^{o}_{FAD}\right)}{2.303RT} \qquad \text{Eq. 2}$$

Similar steps were followed to calculate the $E°_{ASQ/HQ}$ of all the ETFs. However in determining $E°_{OX/HQ}$ from phase 3 of reduction in the presence of PS and SO, the strong absorbances of the dyes at 454 nm interferes with the flavin spectra. Thus, the extent of flavin oxidation was assessed at the isosbestic point of the dye's reduction at 406 nm (for SO dye), where the extinction coefficients of oxidized and reduced dye are equal.

Structural model of WT-*Rpa*ETF

No crystal structure of *Rpa*ETF is available but both subunits have over 40% identity with the corresponding subunits of the *Afe*ETF. Therefore, we generated a structural model of *Rpa*ETF based on the crystallographic coordinates 4KPU.pdb of *Afe*ETF using

Swiss Model (62). The active site residues of *Rpa*ETF are shared by *Afe*ETF, and indeed the coordinates of *Afe*ETF's FAD moieties could be added to the protein model produced by Swiss Model with only minor clashes affecting a few side chains. To eliminate artifacts resulting from amino acid side chain differences, we subjected the initial *Rpa*ETF model to molecular mechanics geometry optimization by energy minimization using CHARMM (63), and then validated the resulting active sites by quantum mechanical molecular mechanical optimization followed by computation of electronic spectra for each of the two flavins using time-dependent density functional theory (TD-DFT) using B3LYP/6-31++G(d,p)(24). The computed OX spectra replicate the differences between the observed spectra of OX ET FAD and Bf FAD, indicating that the optimized flavin binding sites capture the environmental factors and interactions that are most important determinants of the flavin electronic structures.

Data availability

Data will be made available upon reasonable request, made to A.-F. Miller afmill3r2@gmail.com.

Supporting information

This article contains supporting information.

Funding and Acknowledgements.

The authors are grateful to the National Science Foundation for support under awards numbers CLP-1808433 and CLP-2108134. We thank H. D. Duan for providing R165K- and R165H-*Rpa*ETF constructs, T. Creamer for access to the CD spectrapolarimeter, A. Sebesta and B. Gess for maintenance of vital research infrastructure, S. Wang and A. Iyer for access to mass spectrometry, K. Ranguelova for guidance with EPR and M. Ilham.

Conflict of Interest

The authors declare that they have no conflicts of interest with the contents of this article.

References

1. Toogood, H. S., Leys, D., and Scrutton, N. S. (2007) Dynamics driving function : new insights from electron transferring flavoproteins and partner complexes. *FEBS J.* **274**, 5481-5504
2. Toogood, H. S., van Thiel, A., Scrutton, N. S., and Leys, D. (2005) Stabilization of non-productive conformations underpins rapid electron transfer to electron transferring flavoprotein. *J. Biol. Chem.* **280**, 30361-30366
3. Demmer, J. K., Bertsch, J., Oppinger, C., Wohlers, H., Kayastha, K., Demmer, U., Ermler, U., and Muller, V. (2018) Molecular basis of the flavin-based electron-bifurcarting caffeyl-coA reductase reaction. *FEBS Lett.* **592**, 332-342
4. Demmer, J. K., Chowdhury, N. P., Selmer, T., Ermler, U., and Buckel, W. (2017) The semiquinone swing in the bifurcating electron transferring flavoprotein/butyryl-coA dehydrogenase complex from *Clostridium difficile*. *Nat. Commun.* **8**, 1577
5. Thorpe, C. (1991) Electron-Transferring Flavoproteins. in *Chemistry and Biochemistry of Flavoenzymes* (Müller, F. ed.), CRC press, Boca Raton FL. pp 471-486
6. Jones, M., Basran, J., Sutcliffe, M. J., Grossmann, J. G., and Scrutton, N., S,. (2000) X-ray scattering studies of Methylophilus methylotrophus (sp W(3)A(1)) electron-transferring flavoprotein - Evidence for multiple conformational states and an induced fit mechanism for assembly with trimethylamine dehydrogenase. *J. Biol. Chem.* **275**, 21349-21354
7. Roberts, D. L., Frerman, F. E., and Kim, J. J. (1996) Three-dimensional structure of human electron transfer flavoprotein to 2.1-A resolution. *Proc Natl Acad Sci U S A* **93**, 14355-14360
8. Roberts, D. L., Salazar, D., Fulmer, J. P., Frerman, F. E., and Kim, J. J. (1999) Crystal structure of Paracoccus denitrificans electron transfer flavoprotein: structural and electrostatic analysis of a conserved flavin binding domain. *Biochemistry* **38**, 1977-1989
9. Burgess, S. G., Messiha, H. L., Katona, G., Rigby, S. E. J., Leys, D., and Scrutton, N. S. (2008) Probing the dynamic interface between trimethylamine dehydrogenase (TMADH) and electron transferring flavoprotein (ETF) in the TMADH-2ETF complex: Role of the Arg-α237 (ETF) and Tyr-442 (TMADH) residue pair. *Biochemistry* **47**, 5168-5181
10. Dwyer, T. M., Zhang, L., Muller, M., Marrugo, F., and Frerman, F. E. (1999) The functions of the flavin contact residues αArg249 and βTyr16, in human electron transfer flavoprotein. *Biochim. Biophys. Acta.* **1433(1-2)**, 139-152
11. Watmough, N. J., and Frerman, F. E. (2010) The electron transfer flavoprotein: Ubiquinone oxidoreductases. *Biochim. Biophys. Acta* **1797**, 1910-1916
12. Sato, K., Nishina, Y., and Shiga, K. (2003) Purification of electron-transferring flavoprotein from *Megasphaera elsdenii* and binding of additional FAD with an unusual absorption spectrum. *J. Biochem.* **134**, 719-729
13. Garcia Costas, A. M., Poudel, S., Miller, A.-F., J., S. G., Ledbetter, R. N., Fixen, K., Seefeldt, L. C., Adams, M. W., Harwood, C. S., Boyd, E. S., and Peters, J. W. (2017) Defining electron bifurcation in the electron transferring flavoprotein family. *J. Bacteriol.*
14. Sato, K., Nishina, Y., and Shiga, K. (2013) Interaction between NADH and electron-transferring flavoprotein from *Megasphaera elsdenii*. *J. Biochem.* **153**, 565-572

15. Herrmann, G., Jayamani, E., Mai, G., and Buckel, W. (2008) Energy conservation via electron-transferring flavoprotein in anaerobic bacteria. *J. Bacteriol.* **190**, 784-791
16. Weidenhaupt, M., Rossi, P., Beck, C., Fischer, H.-M., and Hennecke, H. (1996) Bradyrhizobium japonicum possesses two discrete sets of electron transfer flavoprotein genes:fixA, fixB and etfS, etfL. *Archives of Microbiology* **165**, 169-178
17. Ledbetter, R. N., Garcia Costas, A. M., Lubner, C. E., Mulder, D. E., Tokmina-Lukaszewska, M., Artz, J. H., Patterson, A., Magnuson, T. S., Jay, Z. J., Duan, H. D., Miller, J., Plunkett, M. H., Hoben, J. P., Barney, B. M., Carlson, R. P., Miller, A.-F., Bothner, B., King, P. W., Peters, J. W., and Seefeldt, L. C. (2017) The electron bifurcating FixABCX protein complex from *Azotobacter vinelandii*: Generation of low-potential reducing equivalents for nitrogenase catalysis. *Biochemistry* **56**, 4177-4190
18. Chowdhury, N. P., Mowafy, A. M., Demmer, J. K., Upadhyay, V., Koelzer, S., Jayamani, E., Kahnt, J., Hornung, M., Demmer, U., Ermler, U., and Buckel, W. (2014) Studies on the mechanism of electron bifurcation catalyzed by electron transferring flavoprotein (Etf) and butyryl-CoA dehydrogenase (Bcd) of *Acidaminococcus fermentans*. *J. Biol. Chem.* **289**, 5145-5157
19. Duan, H. D., Lubner, C. E., Tokmina-Lukaszewska, M., Gauss, G. H., Bothner, B., King, P. W., Peters, J. W., and Miller, A. F. (2018) Distinct flavin properties underlie flavin-based electron bifurcation within a novel electron-transferring flavoprotein FixAB from *Rhodopseudomonas palustris*. *J. Biol. Chem.* **293**, 4688-4701
20. Yang, K. Y., and Swenson, R. P. (2007) Modulation of the redox properties of the flavin cofactor through hydrogen-bonding interactions with the N(5) atom: Role of alpha Ser254 in the electron-transfer flavoprotein from the methylotrophic bacterium W3A1. *Biochem.* **46**, 2289-2297
21. Nitschke, W., and Russell, M. J. (2012) Redox bifurcations: Mechanisms and importance to life now, and at its origin. *Bioessays* **34**, 106-109
22. Schut, G. J., Mohamed-Raseek, N. R., Tokmina-Lukaszewska, M., Mulder, D. E., Nguyen, D. M. N., Lipscomb, G. L., Hoben, J. P., Patterson, A., Lubner, C. E., King, P. W., Peters, J. W., Bothner, B., Miller, A. F., and Adams, M. W. W. (2019) The catalytic mechanism of electron bifurcating electron transfer flavoproteins (ETFs) involves an intermediary complex with NAD+. *J. Biol. Chem.* **294**, 3271-3283
23. Sucharitakul, J., Buttranon, S., Wongnate, T., Chowdhury, N. P., Prongjit, M., Buckel, W., and Chaiyen, P. (2020) Modulations of the reduction potentials of flavin-based electron bifurcation complexes and semiquinone stabilities are key to control directional electron flow. *FEBS J.* **ASAP**, doi:10.1111/febs.15343
24. Mohamed-Raseek, N., Duan, H. D., Mroginski, M. A., and Miller, A. F. (2019) Spectroscopic, thermodynamic and computational evidence of the locations of the FADs in the nitrogen fixation-associated electron transfer flavoprotein. *Chem. Sci.* **10**, 7762-7772
25. Massey, V., and Hemmerich, P. (1980) Active site probes of flavoproteins. *Biochem. Soc. Trans.* **8**, 246-257
26. Lostao, A., Gomez-Moreno, C., Mayhew, S. G., and Sancho, J. (1997) Differential stabilization of the three FMN redox forms by tyrosine 94 and tryptophan 57 in flavodoxin from *Anabaena* and its influence on the redox potentials. *Biochemistry* **36**, 14334-14344

27. Bradley, L. H., and Swenson, R. P. (2001) Role of Hydrogen Bonding Interactions to N(3)H of the Flavin Mononucleotide Cofactor in the Modulation of the Redox Potentials of the *Clostridium beijerinckii* Flavodoxin. *Biochem.* **40**, 8686-8695
28. Talfournier, F., Munro, A. W., Basran, J., Sutcliffe, M. J., Daff, S., Chapman, S. K., and Scrutton, N. S. (2001) alpha Arg-237 in Methylophilus methylotrophus (sp. W3A1) electron-transferring flavoprotein affords approximately 200-millivolt stabilization of the FAD anionic semiquinone and a kinetic block on full reduction to the dihydroquinone. *J Biol Chem* **276**, 20190-20196
29. Peters, J. W., Miller, A. F., Jones, A. K., King, P. W., and Adams, M. W. (2016) Electron bifurcation. *Curr. Opin. Chem. Biol.* **31**, 146–152
30. Sato, K., Nishima, Y., and Shiga, K. (1997) In vitro assembly of FAD, AMP, and the two subunits of electron-transferring flavoprotein: an important role of AMP related with the conformational change of the apoprotein. *J. Biochem.* **121**, 477-486
31. Kayastha, K., Vitt, S., Buckel, W., and Ermler, U. (2021) Flavins in the electron bifurcation process. *Arch. Biochem. Biophys.*, 108796
32. Vigil, J., W., Niks, D., Franz-Badur, S., Chowdhury, N., Buckel, W., and Hille, R. (2021) Spectral deconvolution of redox species in the crotonyl-CoA-dependent NADH:ferredoxin oxidoreductase from *Megasphaera elsdenii*. A flavin-dependent bifurcating enzyme. *Arch. Biochem. Biophys.* **701**, 108793
33. Stanley, R. J. (2001) Advances in flavin and flavoprotein optical spectroscopy *Antiox Redox Sign* **3**, 847-866
34. Kar, R. K., Chasen, S., Mroginski, M. A., and Miller, A. F. (2021) Tuning the quantum chemical properties of flavins via modification at C8. *J. Phys. Chem. B* **125**, 12654–12669
35. Yagi, K., Ohishi, N., Nishimoto, K., Choi, J. D., and Song, P.-S. (1980) Effect of hydrogen bonding on electronic spectra and reactivity of flavins. *Biochemistry* **19**, 1553-1557
36. Cerda, J. F., Koder, R. L., Jr., Lichtenstein, B. R., Moser, C. M., Miller, A.-F., and Dutton, P. L. (2008) Hydrogen Bond-Free Flavin Redox Properties: Managing Flavins in Extreme Aprotic Solvents. *Org. Biomol. Chem* **6**, 2204-2212
37. Mayhew, S. G. (1999) The Effects of pH and Semiquinone Formation on the Oxidation-Reduction Potentials of Flavin Mononucleotide: A Reappraisal. *Eur. J. Biochem.* **265**, 698-702
38. Massey, V. (1991) A simple method for determination of redox potentials. in *Flavins and flavoproteins.* (Curti, B., Ronchi, S., and Zanetti, G. eds.), Walter de Gruyer, Berlin. pp 59-66
39. Clark, W. M. (1960) *Oxidation-Reduction Potentials of Organic Systems*, Williams and Wilkins, Baltimore MD
40. Massey, V., and Palmer, A. G. (1962) Charge transfer complexes of lipoyl dehydrogenase and free flavins. *J. Biol. Chem.* **237**, 2347-2358
41. He, T.-F., Guo, L., Guo, X., Chang, C.-W., Wang, L., and Zhong, D. (2013) Femtosecond Dynamics of Short-Range Protein Electron Transfer in Flavodoxin. *Biochemistry* **52**, 9120-9128
42. Abramovitz, A. S., and Massey, V. (1976) Interaction of phenols with old yellow enzyme. *J. Biochel. Chem.* **251**, 5327-5336

43. Augustin, P., Toplak, M., Fuchs, K., Gerstmann, E. C., Prassl, R., Winkler, A., and Macheroux, P. (2018) Oxidation of the FAD cofactor to the 8-formyl-derivative in human electron-transferring flavoprotein. *J. Biol. Chem.* **293**, 2829-2840
44. Robbins, J. M., Geng, J., Barry, B. A., Gadda, G., and Bommarius, A. S. (2018) Photoirradiation generates an ultrastable 8-formyl FAD semiquinone radical with unusual properties in formate oxidase. *Biochemistry* **57**, 5818-5826
45. Robbins, J. M., Souffrant, M. G., Hamelberg, D., Gadda, G., and Bommarius, A. S. (2018) Enzyme-mediated conversion of flavin adenine dinucleotide (FAD) to 8-formyl FAD in formate oxidase results in a modified cofactor with enhanced catalytic properties. *Biochem* **56**, 3800-3807
46. Schuman, M., and Massey, V. (1971) Purification and characterization of glycolic acid oxidase from pig liver. *Biochim Biophys Acta* **227**, 500-520
47. Macheroux, P., Massey, V., and Thiele, D. J. (1991) Expression of spinach glycolate oxidase in *Saccharomyces cerevisia*e: purification and characterization. *BIochem.* **30**, 4612-4619
48. Ku, H.-K., Lim, H.-M., Oh, K.-H., Yang, H.-J., Jeong, J.-S., and Kim, S.-K. (2013) Interpretation of protein quantitation using the Bradford assay: Comparison with two calculation models. *Anal. Biochem.* **434**, 178-180
49. Jang, M.-H., Scrutton, N. S., and Hille, R. (2000) Formation of W3A1 Electron-transferring Flavoprotein (ETF) Hydroquinone in the Trimethylamine Dehydrogenase·ETF Protein Complex. *J. Biol. Chem.* **275**, 12546-12552
50. Sucharitakul, J., Buckel, W., and Chaiyen, P. (2021) Rapid kinetics reveal surprising flavin chemistry in the bifurcating electron transfer flavoprotein from *Acidaminococcus fermentans*. *J. Biol. Chem.* **296**, 100124
51. Lehman, T. C., and Thorpe, C. (1992) A new form of mammalian electron transfer flavoprotein. *Arch Biochem. Biophys.* **292**, 594-599
52. Mayhew, S. G., Whitfield, C. D., Ghisla, S., and M., S.-J. (1974) Identification and properties of new flavins in electron-transferring flavoprotein from *Peptostreptococcus elsdenii* and pig-liver glycolate oxidase. *Eur, J. Biochem.* **44**, 570-591
53. Ghisla, S., Massey, V., and Mayhew, S. G. (1976) Studies on the active centers of flavoproteins: Binding of 8-hydroxy-FAD and 8-hydroxy-FMN to apoproteins. in *Flavins and Flavoproteins* (Singer, T. P. ed.), Elsevier, Amsterdam. pp 334-340
54. O'Neill, H., Mayhew, S. G., and Butler, G. (1998) Cloning and analysis of the genes for a novel electron-transferring flavoprotein from *Megasphaera elsdenii*. *J Biol Chem* **273**, 21015-21024
55. Chowdhury, N. P., Kahnt, J., and Buckel, W. (2015) Reduction of ferredoxin or oxygen by flavin-based electron bifurcation in Megasphaera elsdenii. *FEBS J.* **282**, 3149-3160
56. Sato, K., Nishina, Y., and Shiga, K. (1993) Electron-transferring flavoprotein has an AMP-binding site in addition to the FAD-binding site. *J Biochem* **114**, 215-222
57. DuPlessis, E. R., Rohlfs, R. J., Hille, R., and Thorpe, C. (1994) Electron-transferring flavoproteins from pig and the methylotrophic bacterium W3A1 contains AMP as well as FAD. *Biochem. Mol. Biol. Int.* **32**, 195-199
58. Feng, X., Schut, G. J., Lipscomb, G., Li, H. Y., and Adams, M. W. W. (2021) Cryoelectron microscopy structure and mechanism of the membrane-associated electron-bifurcating flavoprotein Fix/EtfABCX. *Proc. Natl. Acad. Sci. U. S. A.* **118**, e2016978118

59. Duan, H. D., Mohamed-Raseek, N., and Miller, A. F. (2020) Spectroscopic evidence for direct flavin-flavin contact in a bifurcating electron transfer flavoprotein. *J. Biol. Chem.* **295**, 12618-12634
60. Yousafzai, F. K., and Eady, R. R. (2002) Dithionite Reduction Kinetics of the Dissimilatory Copper-containing Nitrite Reductase of Alcalegenes xylosoxidans : The SO radical binds to the substrate binding type 2 copper site before the type 2 copper is reduced. *J. Biol. Chem.* **277**, 34067-34073
61. Miller, A. F., Duan, H. D., Varner, T. A., and Mohamed-Raseek, N. (2019) Reduction midpoint potentials of bifurcating electron transfer flavoproteins. *Meth. Enzymol.* **620**, 365-398
62. Waterhouse, A., Bertoni, M., Bienert, S., Studer, G., Tauriello, G., Gumienny, R., Heer, F. T., de Beer, T. A. P., Rempfer, C., Bordoli, L., Lepore, R., and Schwede, T. (2014) SWISS-MODEL: homology modelling of protein structures and complexes. *Nucleic Acids Res.* **46**, W296-W303
63. Huang, J., Rauscher, S., Nawrocki, G., Ran, T., Feig, M., de Groot, B. L., Grubmüller, H., and MacKerell, A. D., Jr. . (2017) CHARMM36m: an improved force field for folded and intrinsically disordered proteins. *Nat. Methods.* **14**, 71-73
64. Lei, C., Zhang, Z., Liu, H., Kong, J., and Deng, J. (1996) Biosensoring of hydrogen peroxide using new methylene blue N incorporated in a montmorillonite-modified horseradish peroxidase immobilization matrix as an electron shuttle. *Analytica Chimica Acta* **332**, 73-81
65. Oja, S. M., Guerrette, J. P., David, M. R., and Zhang, B. (2014) Fluorescence-enabled electrochemical microscopy with dihydroresorufin as a fluorogenic indicator. *Analytical Chemistry* **86**, 6040-6048
66. Twigg, R. S. (1945) Oxidation-Reduction Aspects of Resazurin. *Nature* **155**, 401-402
67. Husain, M., Stankovich, M. T., and Fox, B. G. (1984) Measurement of the oxidation-reduction potentials for one-electron and two-electron reduction of electron-transfer flavoprotein from pig liver. *The Biochemical journal* **219**, 1043-1047
68. Griffin, K. J., Dwyer, T. M., Manning, M. C., Meyer, J. D., Carpenter, J. F., and Frerman, F. E. (1997) alphaT244M mutation affects the redox, kinetic, and in vitro folding properties of Paracoccus denitrificans electron transfer flavoprotein. *Biochemistry* **36**, 4194-4202
69. Pettersen, E. F., Goddard, T. D., Huang, C. C., Couch, G. S., Greenblatt, D. M., Meng, E. C., and Ferrin, T. E. (2004) UCSF Chimera - a visualization system for exploratory research and analysis. *J. Comput. Chem.* **25**, 1605-1612
70. Vdovin, A., Slenczka, A., and Dick, B. (2013) Electronic spectroscopy of lumiflavin in superfluid helium nanodroplets. *Chem. Phys.* **422**, 195-203

Figure Captions

Figure 1. Structure of Bf ETF in the B-like (closed) conformation (A), interactions with two target Args (B, C) and essence of flavin-based bifurcation reaction (D). A: Model of *Rpa*ETF based on coordinates 4KPU.pdb generated using Swiss Model (62) and then subjected to geometry optimization (63) and validated by computation of electronic spectra for each of the two flavins. The 'A' subunit is in blue and the 'B' subunit is in grey, domains are also indicated (24). B: Disposition of Arg-273 adjacent to the ET flavin bound in domain II of EtfA, note that Arg-273 derives from EtfA. C: disposition of R165 perpendicular to the Bf flavin, interacting with both it and a stretch of peptide backbone from the other subunit. Arg-165 derives from EtfA (blue Cα) whereas the stretch of peptide derives from EtfB (grey Cα), and the Bf flavin resides in the interface between domains I and III. All molecular graphics images were generated using Chimera (69). D: Depiction of flavin's role in electron bifurcation, accepting a hydride equivalent to two electrons (2e) from NADH, transmitting one electron (1e) to a higher-energy electron carrier (here ferredoxin, Fd) as paid for by exergonic transfer of the other electron to quinone via other carriers (here ET flavin and FixCX). The Bf flavin is indicated by the fused green hexagons. Note that two NADH-consuming turnovers are required to supply the two reducing equivalents needed to convert one quinone (Q) to a quinol (QH_2).

Figure 2. Comparison of deconvoluted absorbance spectra of ET FAD (A) and Bf FAD (B) in the different variants. The signals of the Bf flavins (B) display larger separation between band I near 450 nm and band II near 380 nm, as well as more prominent shoulders on band I that are attributed to transitions to and from different vibrational substates of the π and π* electronic states involved in the transition (70). Comparisons of spectra in non-polar solvents ± hydrogen bonding partners demonstrate that stronger longer-lived hydrogen bonds correlate with increased strength for such features (36). Reductive titrations of WT and variants were used to deconvolute the ET and Bf FAD spectra. The deconvolution process is described in the Experimental Procedures section and Supporting Figure S2. Vertical offsets were applied to facilitate comparisons between spectra. Samples were either 30 μM, or their spectra were scaled to produce amplitude corresponding to 30 μM. ET FAD spectra were offset by 0.0, 0.15, 0.25, 0.35, 0.45, .0.55 for R165H-, R165K-, R273H-, R273A-, R273K- and WT-*Rpa*ETF, respectively. For Bf FAD spectra, vertical offsets were 0.15, 0.3, 0.4, 0.55, for R273H-, R273A-, R273K- and WT-*Rpa*ETF, respectively.

Figure 3. Three phases of stepwise reduction of R165K-*Rpa*ETF with Ti(III) citrate. Visible spectra observed at each step of reduction, with the first spectrum of fully oxidized R165K in purple, the spectrum at the end of phase 1 in bright green (maximum population of ASQ), the spectrum at the end of phase 2 in light orange and the fully reduced endpoint after phase 3 in dark brown. Inset shows a plot of the A_{374} vs. A_{456}, revealing the three different slopes that distinguish the three phases of reduction. The first spectrum gives rise to the point furthest to the right and the point corresponding to the last spectrum is in the lower left. In all phases A_{456} decreases, but in phase 1, growth of ASQ more than compensates for loss of OX at A_{374}. In phase 2 the loss of this stronger absorbance makes A_{374} drop steeply, whereas in phase 3 A_{374} reflects loss of the weaker OX signal and its replacement by weaker still HQ. Data for a 22 μM sample are shown.

Figure 4. Log/log plots of populations present during co-reduction of ETF and dye in reductive titration of R165K-*Rpa*ETF. Log([oxidized FAD]/ [reduced FAD]) for the flavins of R165K-*Rpa*ETF is plotted vs. the analogous quantity for the dye, showing linear behavior in each of the three phases of reduction, consistent with the Nernst equation. The slopes near 0.5 for phases 1 and 2 are consistent with 1e events and the slope near 1.0 for phase 3 indicates a 2e event, because all the dyes used underwent 2e reduction, see Experimental Procedures.

Figure 5. Reductive titrations of R165H with NADH or dithionite. A: Spectra observed in the course of reduction with sodium dithionite (DT). B: spectra observed during reduction by NADH. The inset in A provides the absorbance at 374 nm vs. that at 450 nm. A_{374} reports on ASQ formation and then consumption as the ETF is reduced (see also inset to Figure 3).

Figure 6. Spectra of ETF R165-*Rpa*ETF variants and their released flavins. Spectra scaled to correspond flavin concentrations of 30 μM and compared for (A) ETF variants and (B) cofactors released from them. R165H- and R165Q-*Rpa*ETF purified and maintained at pH 8 are compared to T94,97A-*Rpa*ETF purified and maintained at pH 9, revealing a sharp feature near 425 nm. This is attributed to the flavin itself rather than the environment since displacement and replacement with fresh FAD greatly diminishes it ('reconstitution'). Nevertheless, all spectra retain absorbance at long wavelengths. Spectra of released flavins (B) confirm that the flavin itself sustains chemical modification in R165Q-*Rpa*ETF at pH 8, similar to that seen in T94,97A-*Rpa*ETF at pH 9.

Figure 7. Extended electrostatically polarized network of H-bonds bridging the domain interface and mediated by the conserved peptide zipper. Figure is based on the crystal structure of *Afe*ETF, 4KPU.pdb (18). *Rpa*ETF residue numbering is used, for consistency with text, but in *Afe*ETF the EtfA residues shown are Arg-146, Ala-129 (in blue), and the EtfB residues shown are Gly-123, Asp-124, Thr-125 and Ala-126 (in grey).

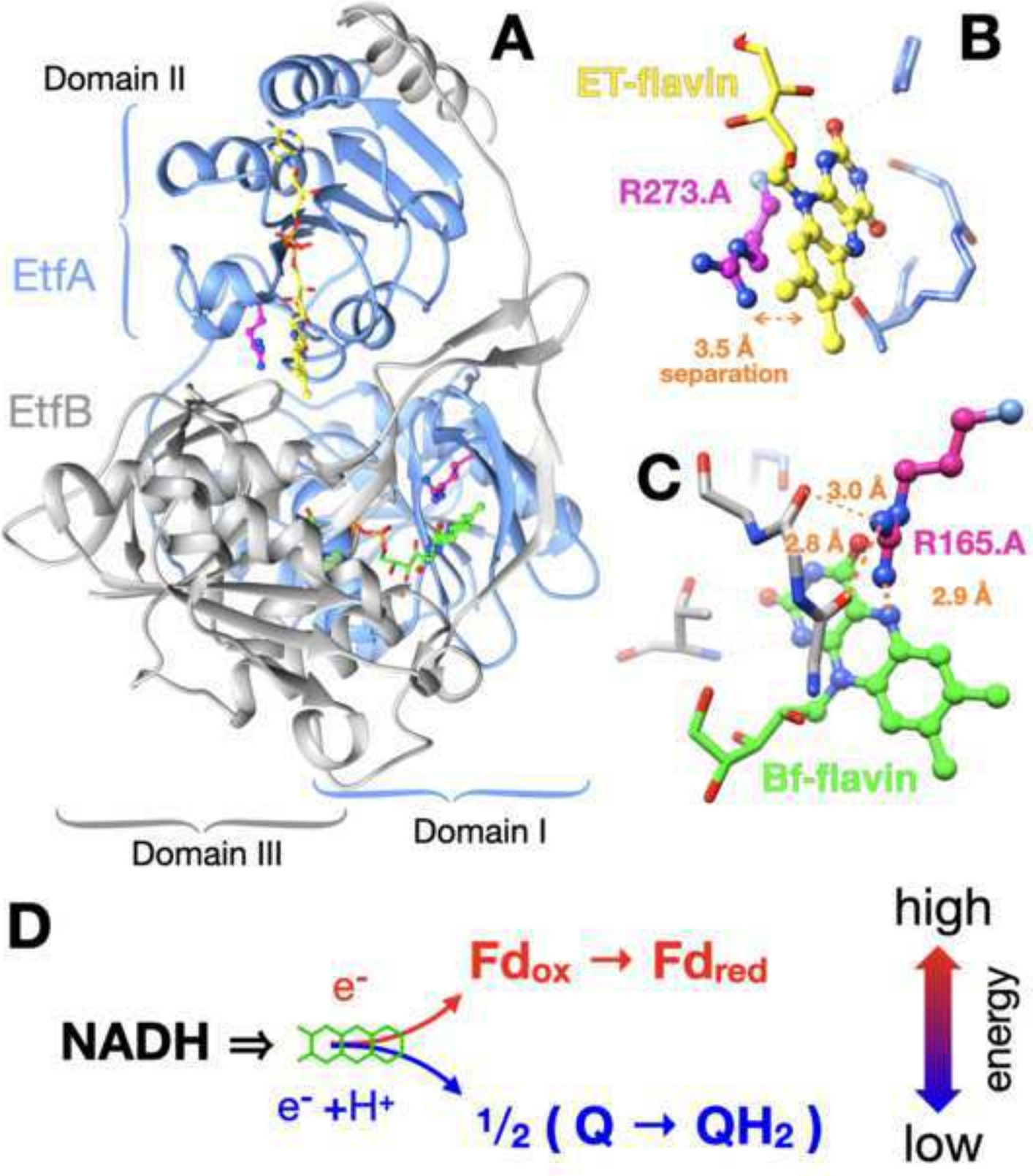

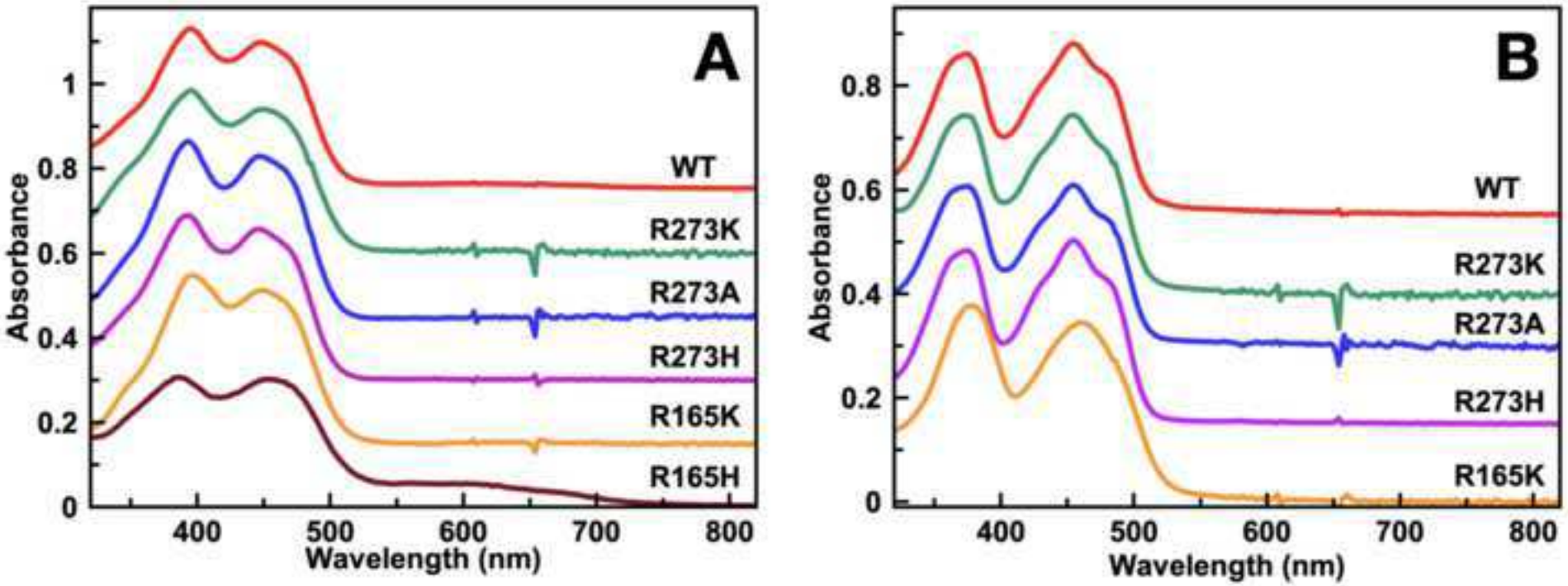

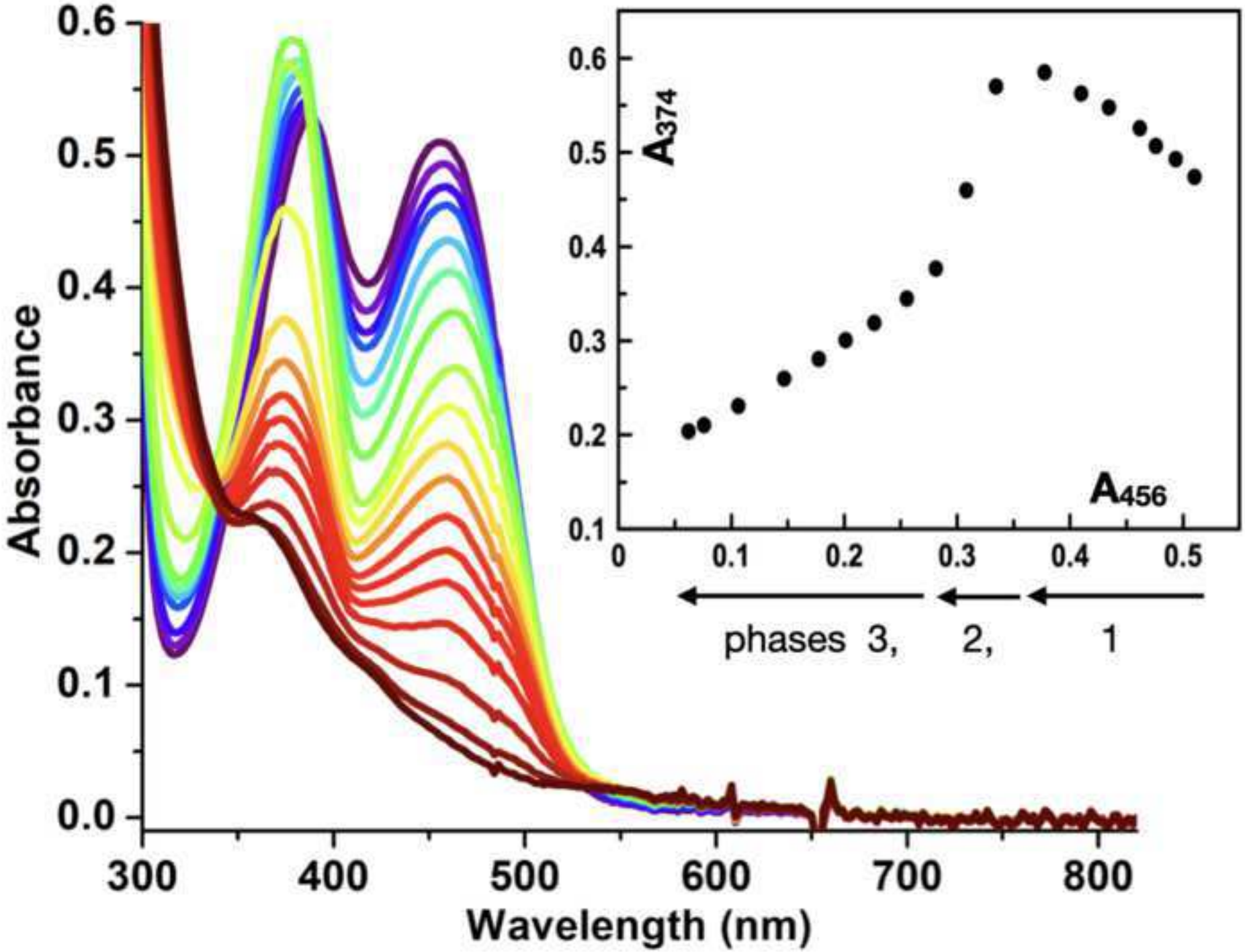

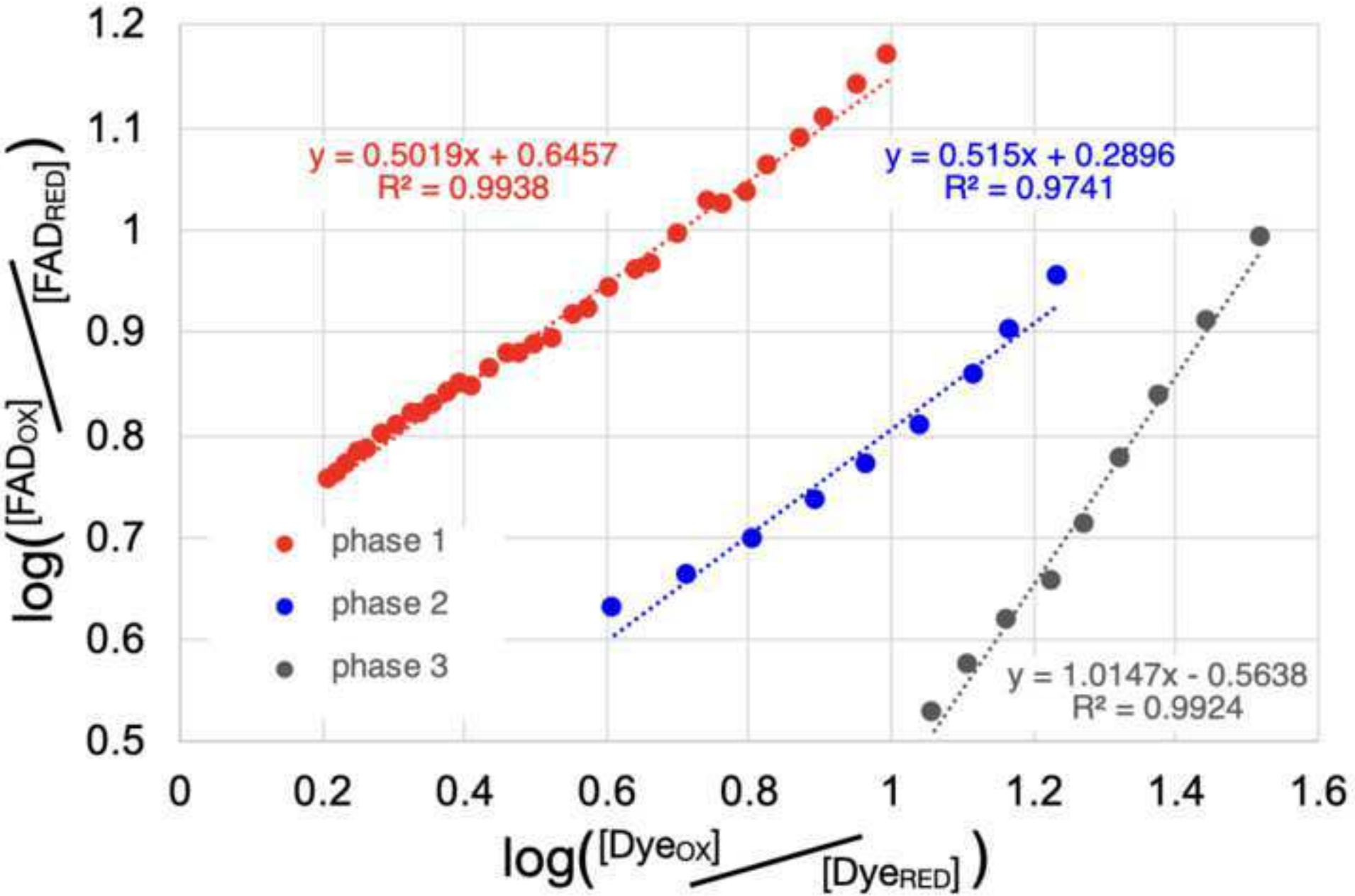

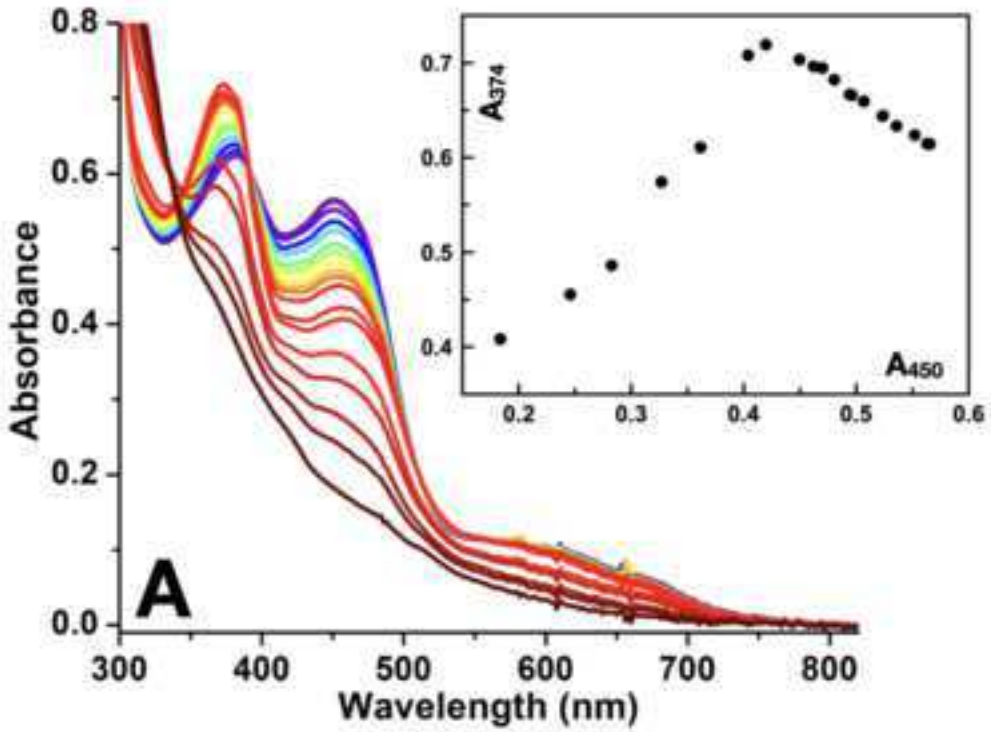

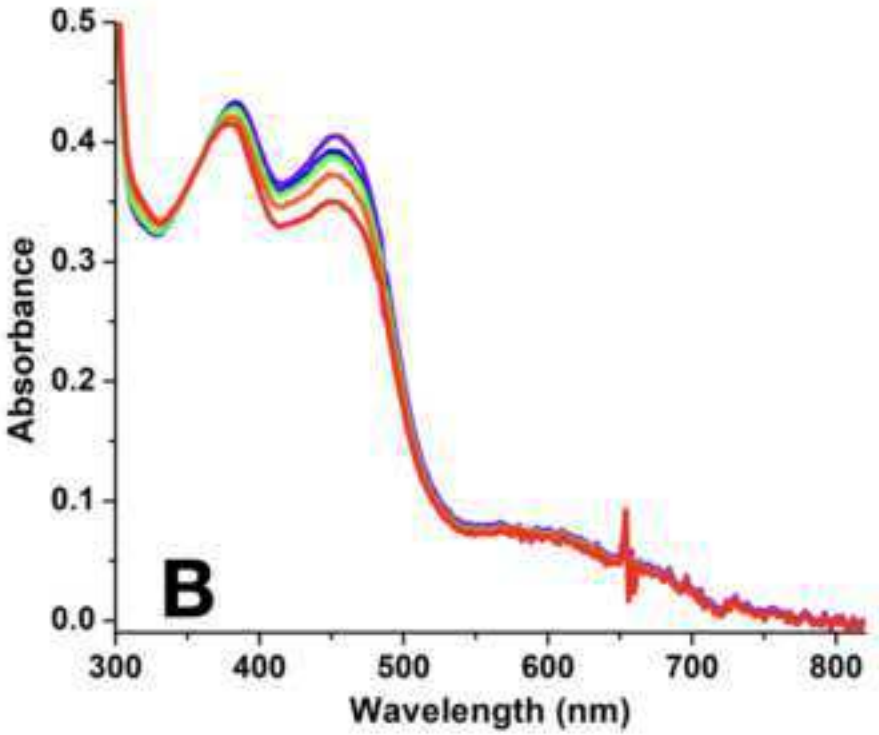

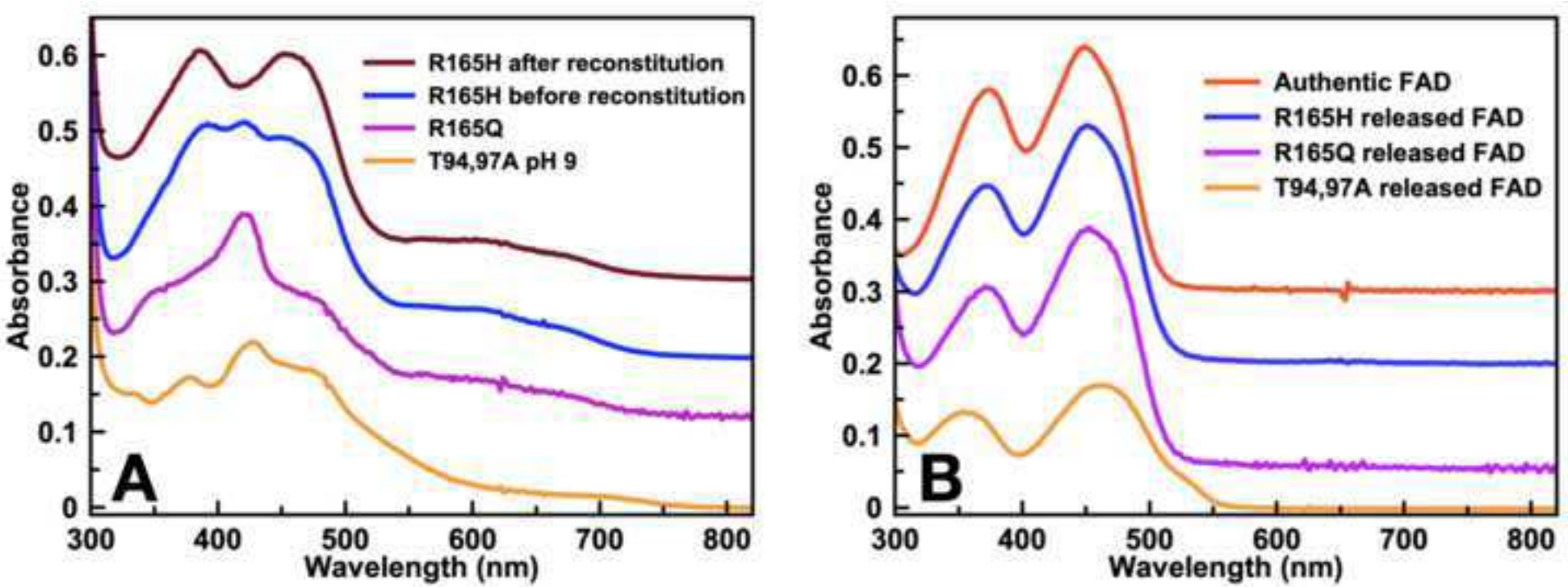

Main Figure (High Resolution)

Click here to access/download;Main Figure (High Resolution);HighResFig7_Zipper.tiff

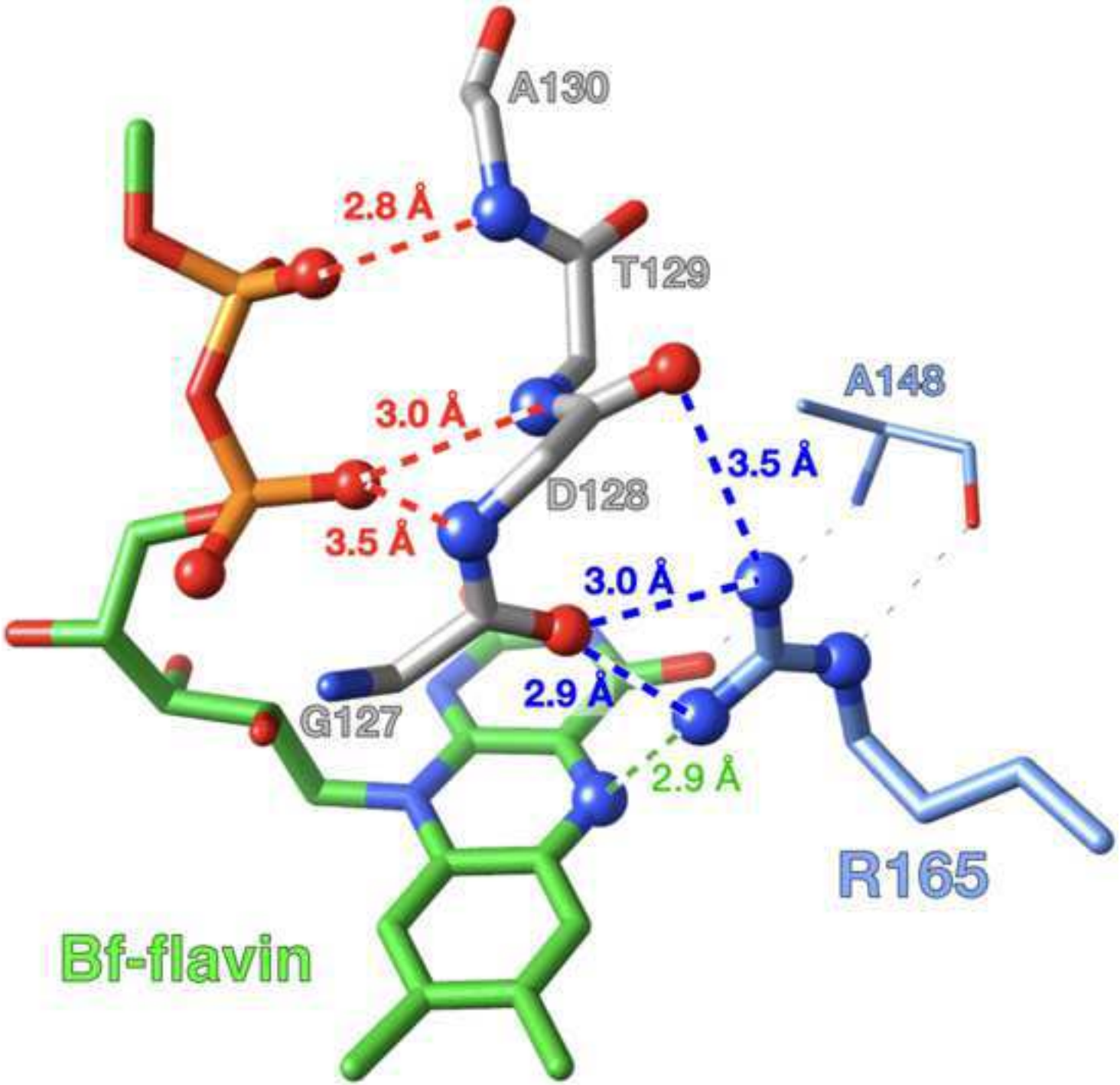

Table1: Flavin contents and thermal stabilities.

*Rpa*ETF Variant	FAD content/dimer	T_m (°C)[a]
WT	2.00 ± 0.00[b]	46 ± 2
R273A	2.04 ± 0.06	44 ± 0
R273H	2.03 ± 0.04	44 ± 0
R273K	2.09 ± 0.07	44 ± 0
R165K	2.00 ± 0.00	44 ± 0
R165H	0.88 ± 0.12	40 ± 2

[a] T_m values were measured on 17-30 μM ETF in 20 mM working buffer with 200 mM KCl and 10% (w/v) glycerol at pH 8.

[b] Standard deviations of 0.00 indicate that the two independent trials gave the same value.

Table 2: Comparison of absorption maxima of individual flavins in each variant, at pH 8.

*Rpa*ETF Variant	ET FAD			Bf FAD		
	Band I (near 450 nm) (±2 nm)	Band II (near 380 nm) (±2 nm)	Band Height Ratio II/I	Band I (near 450 nm) (±2 nm)	Band II (near 380 nm) (±2 nm)	Band Height Ratio II/I
WT	448	394	1.04	454	374	0.98
R273K	450	396	1.06	454	374	0.99
R273A	446	392	1.05	454	374	0.99
R273H	446	394	1.05	454	374	0.96
R165K	448	396	1.07	460	378	1.09
R165H	452	386	1.01	N/A	N/A	N/A

Table 3. Maximum population of ASQ in different variants.

*Rpa*ETF Variant	ASQ_{max}	K_{sq}	$E°_{OX/ASQ}$ - $E°_{ASQ/HQ}$ (mV)[a]
WT	0.84 ± 0.0[b,c]	110	122
R273K	0.84 ±0.0[c]	110	127
R273A	0.52±0.03[c]	4.69	40
R273H	0.71 ±0.00[d]	23.98	82
R165K	0.84 ± 0.0[c]	110	125
T94,97A	0.74 ± 0.0[c]	32.4	89

[a] uncertainties are ≤5 mV, See supporting Table S1.

[b] Reference value, calculated from the separation between *E*°s determined here.

[c] Two independent repetitions.

[d] Both sets of slopes produced the same values.

Table 4: Effects on E° of replacing the arginine residues.

*Rpa*ETF Variant	Flavin content	$E°_{OX/ASQ}$	$E°_{ASQ/HQ}$	$E°_{OX/HQ}$ (mV)
WT	2	-61± 3 a	-182 ± 2[c]	-273 ± 5 (n=2)[d]
R273K	2	-69 ± 4[a]	-185 ± 5[c]	-273 ± 5 (n=2) [d]
R273H	2	-119 ± 2 [b]	-201 ± 2[c]	-310 ± 2 (n=2) [e]
R273A	2	-137[b]	-178 ± 2[c]	-313 ± 2 (n=2) [e]
R165K	2	-67.6[a]	-182 ± 2[c]	-271 ± 5 (n=2) [d]

[a] $E°_{OX/ASQ}$ was measured by co-reduction with new methylene blue (NMB) with the calculated potential of -51 mV ($E°'$ = -21 mV, 2e/H^+ at pH 7) (64) and λ_{max} of NMB is at 632 nm.

[b] Determined by co-reduction with resorufin, RS ($E°'$ = -51 mV, 2e/2H^+ at pH 7, calculated $E°$ = -111 mV pH 8) (65,66) using A_{572} nm for RS.

[c] Determined by co-reduction with Nile blue, NB ($E°'$ = -116 mV, 2e/H^+ at pH 7, calculated $E°$ = -146 mV pH 8) (19,61). λ_{max} of NB is at 636 nm

[d] Determined by co-reduction with phenosafranin (PS, $E°'$ = -252 mV, 2e/H^+ at pH 7, calculated $E°$ = -282 mV pH 8) (19,61)

[e] Safranin O, $E°'$ = -289 mV, 2e/H^+ at pH 7, calculated $E°$ = -319 mV pH 8)(22,61)

Table 5: pH dependence of flavin occupancy in Bf site variants.

RpaETF Variant	FAD content (per dimer, at pH 8)	AMP content (per dimer, at pH 8)	FAD content (per dimer, at pH 9)
WT	2	0.0	2
R165K	2	0.0	2
R165H	0.9 ± 0.1	0.2 ± 0.0	1.6
R165Q	0.26 ± 0.00	0.8 ± 0.2	1

Table 6: Comparison of E°'s of 1 and 2-FAD systems[a].

System	Flavin content	*E°'$_{OX/ASQ; ASQ/HQ; OX/HQ}$* (mV)	Ref.
Free flavin	N/A	-313; -101; -207	(37)
2-FAD ETFs			
*Pae*ETF	2	+33; -94; -285	(22)
*Afe*ETF	2	+134; -36; -249	(23)
WT *Rpa*ETF	2	-47; -83; -223 -61; -122; -243	(19,24) This work
R273K-*Rpa*ETF	2	-69, -125, -243	This work
R273H-*Rpa*ETF	2	-119, -141, -280	This work
R273A-*Rpa*ETF	2	-137, -118, -283	This work
R165K-*Rpa*ETF	2	-67.6, -122, -241	This work
T94,97A-*Rpa*ETF	1	-7, -96	This work
*Mel*ETF	2	+81; -136; -279	(14)
1-FAD ETFs			
T94,97A *Rpa*ETF	1	-7; -96	(24), This work
*Mme*ETF WT	1	+153; <-250; N.A.	(9,28)
*Mme*ETF αR237A	1	-43; -31; N.A.	(9,28)
*Mme*ETF αR237K	1	-62; <-250; N.A.	(9)
αR237C	1	-57; -145; N.A.	(9)
αR237E	1	-59; -199; N.A.	(9)
Human WT	1	+22; -42; N.A.	(10)
Human αR249K	1	-39: -124; N.A.	(10)
Pig liver *Sus domesticus*	1	+4; -20; N.A.	(67)
Paracoccus denitrificans	1	-6; -36; N.A.	(68)

[a] values are adjusted to pH 7, see also (14,19)